The Design and Construction of a 20” x 20” Mach 2.0 Blowdown Wind Tunnel to Characterize the Lift and Drag of Irregularly Shaped Fragments

Christopher W. Larson

Thesis submitted to the Faculty of the Virginia Polytechnic Institute and State University in partial fulfillment of the requirements for the degree of

Master of Science

in

Mechanical Engineering

Wing F. Ng, Chair

Clinton L. Dancey, Co-Chair

Thomas E. Diller

April 25, 2011

Blacksburg, VA

Keywords: Supersonic Wind Tunnel, Irregularly Shaped Fragments, Lift and Drag Force

The Design and Construction of a 20” x 20” Mach 2.0 Blowdown Wind Tunnel to Characterize the Lift and Drag of Irregularly Shaped Fragments

Christopher W. Larson

(Abstract)

A supersonic wind tunnel, with a 20” x 20” test section cross sectional area, was designed and constructed at the Techsburg Wind Tunnel Facility in order to determine the lift and drag on irregularly shaped fragments in supersonic flow. Prior to beginning the wind tunnel design process, a blowdown analysis model was created in order to determine the influence of a number of parameters on tunnel run time and test gas properties throughout the tunnel circuit. The design of the settling chamber, test section, supersonic nozzles, diffuser, and exhaust are presented in this thesis. Diffuser performance has a large influence on wind tunnel efficiency and run time. Therefore, significant efforts should be taken in order to attain the highest possible pressure recovery within the diffuser. The design of wind tunnel components, as well as their stress analysis, was conducted using SolidWorks. The control valve and silencer were sized and selected for the expected tunnel operating conditions. Since the control valve tends to encompass a significant portion of the overall tunnel cost, care must be taken to ensure it has a large enough flow capacity to produce the desired test conditions. Also, attempts must be made to accurately predict the total pressure loss through the silencer, since this loss can have a large impact on the total pressure ratio necessary to produce the design Mach number. Upon completion of the design process, the supersonic wind tunnel was assembled, and shakedown testing was conducted. During shakedown testing it was determined that the wind tunnel was capable of producing Mach 2 flow in the test section. Following shakedown testing, a flow survey was conducted in order to ensure uniform Mach number flow exists throughout the region occupied by the fragments. Based on the flow survey it was determined that within the middle 60% of the test section, the average Mach number was 1.950 and varied by only 0.56% within this region. Two irregularly shaped fragments were tested at Mach 2 flow, over an effective 360° pitch sweep, with wind tunnel runs performed every 10 degrees. Based on the measured force data for both fragments, the lift appeared to follow a sinusoidal curve, with minimum values at 0, 90, and 180° balance pitch angle, and maximum values occurring around 45 and 135° pitch angle. The drag force was observed to follow a gradual curve with minimum values at 0 and 180° balance pitch angle, as expected since the fragment presented area is generally least in this orientation. The maximum drag was found to occur at a balance pitch angle of 90°, once again as expected since the fragment presented area is generally greatest at this angle. It was also observed that the fragment drag tended to be greater for a fragment orientation which places the concave side of the fragment into the direction of the flow.

Acknowledgments

I would like to thank Dr. Wing Ng for giving me the opportunity to work on this project, and for the support and patience he has given me throughout its entirety. Even though this project had its share of problems and difficulties, Dr. Ng continued to motivate and encourage me not to give up. I would also like to thank Dr. Clint Dancey and Dr. Thomas Diller for serving on my advisory committee.

I would especially like to thank Matthew Langford from Techsburg, my mentor, and the Senior Research Engineer on the project. Without the continued help and advice I received from Matt, this project would not have been possible. I would also like to thank the entire engineering staff at Techsburg, all of whom provided help and insight throughout the project. Thanks to Sarah Tweedie for creating the data acquisition and control program for the wind tunnel. Thanks to Zack Boor for his advice, fork lift driving, and help in wind tunnel assembly. Thank you to Stephen Guillot and Jon Fleming for their insight and help over the course of the project. Also, I would like to thank Gary Dudding, and Greg Whitaker, and all of the machine shop for machining a number of wind tunnel parts.

Lastly, I would like to thank my parents, Brian and Susan, my brother Peter, and all of my friends for their continued support. If it weren't for the support of my parents, and the values they instilled in me, I would not be where I am today.

Table of Contents

Index of Figures

Index of Tables

Index of Equations

Nomenclature

Acronyms

CAD	Computer Aided Design
CFD	Computational Fluid Dynamics

Variables

A_{TS}	Test Section Cross Sectional Area
A_2^*	Diffuser Throat Area
A/A^*	Choked Flow Area Ratio
C_P	Subsonic Diffuser Pressure Recovery Coefficient
F_{xe}	Force in x-direction (Earth Fixed Coordinate System)
F_{ye}	Force in y-direction (Earth Fixed Coordinate System)

F_{ze}	Force in z-direction (Earth Fixed Coordinate System)
h	Test Section Half-Span Height
K	Screen Pressure Drop Coefficient
L/d	Model Length to Thickness Ratio
L_{max}	Maximum Allowable Model Length
$\dot{m}$	Mass Flow Rate
$\dot{m}_1$	Initial Mass Flow Rate
$\dot{m}_2$	Mass Flow Rate After a Given Amount of Time
M	Mach Number
M_{TS}	Test Section Mach Number
M_1	Upstream Mach Number
M_2	Downstream Mach Number
$\mathcal{M}$	Mass of Air in the Storage Tanks
$\mathcal{M}_1$	Initial Mass of Air in the Storage Tanks
$\mathcal{M}_2$	Mass of Air in the Storage Tanks After a Given Amount of Time
p_{amb}	Ambient Pressure
p_{TS}	Test Section Static Pressure
p_0	Stagnation Pressure
p_{0_TS}	Test Section Stagnation Pressure
p_{0_tank}	Air Storage Tank Stagnation Pressure
$p_{0\_tank\_init}$	Test Section Stagnation Pressure
p_{0_SL}	Silencer Total Pressure Loss
p_{01}	Upstream Stagnation Pressure
p_{02}	Downstream Stagnation Pressure
r	Diffuser Pressure Recovery

R	Gas Constant
T	Static Temperature
T_{TS}	Test Section Static Temperature
T_0	Stagnation Temperature
T_{0_TS}	Test Section Stagnation Temperature
T_{0_tank}	Air Storage Tank Stagnation Temperature
T_{01_tank}	Initial Air Storage Tank Stagnation Temperature
T_{02_tank}	Air Storage Tank Stagnation Temperature After a Given Amount of Time
V	Velocity
$\mathcal{V}$	Air Storage Tank Volume

Greek

α	Model Angle of Attack
γ	Specific Heat Ratio
θ	Shockwave Angle
μ	Angle of the Shock Reflection
ρ	Static Density
ρ_{TS}	Test Section Static Density
ρ_0	Air Storage Tank Stagnation Density
ρ_{01}	Initial Air Storage Tank Density
ρ_{02}	Air Storage Tank Density After a Given Amount of Time

Chapter 1.0: Introduction

1.1: Background and Motivation

The flight dynamics and trajectory of a fragment resulting from an explosion or high speed impact can be modeled with knowledge of the gravity, fragment area ratios, mass, velocity, air density, wind speed, and lift and drag coefficient. The lift and drag coefficient of a fragment is dependent on its shape and Mach number. However, since fragments resulting from explosions tend to be very irregular in shape, as can be seen in Figure 1.1 below, each will have its own relationship between lift/drag and orientation. Therefore, in order to improve the accuracy of models which predict fragment trajectories, as well as validate computational fluid dynamics simulations, experimental testing of fragments in a wind tunnel is necessary to determine their individual lift and drag coefficients. Wind tunnel tests of irregular fragments have been previously performed, however most were conducted at low Mach number, subsonic speeds. Fragments produced from an explosion or high speed impact have very high initial velocities in the supersonic range. Since the lift and drag coefficients on standard shapes differ significantly from subsonic to supersonic flight, it can be assumed that the coefficients on irregularly shaped fragments will differ as well.

Figure 1.1. Examples of irregularly shaped fragments.

In addition to measuring aerodynamic force and moment parameters on an object or model, supersonic wind tunnels are used to gather information over a broad spectrum of topics such as heat transfer, ablation and material properties, internal flow dynamics, the influence of propulsion integration, and propulsion system operation. Current applications requiring the use

of supersonic facilities include shuttle and reentry vehicles, aircraft designed for supersonic flight, high speed missiles, and fundamental physics and CFD validation. The following section provides a summary of a few publications on the topics of fragment drag coefficient and supersonic wind tunnel design.

1.2: Previous Research

1.2.1: Drag Coefficients for Irregular Fragments

McCleskey (1988) conducted experimental testing on 96 fragments in the vertical wind tunnel at the U.S. Army Chemical Research, Development and Engineering Center in Aberdeen, Maryland. The purpose of the experimental tests was to try and determine some sort of correlation between drag coefficient and the characteristics of irregular fragments. These correlations could then be used in order to decrease uncertainties associated with trajectory calculations in a computer model which predicts fragment hazards for specified targets. Measurements were made for each fragment, and included linear maximum length, width, and thickness, presented areas, and moment of inertia. During wind tunnel testing, each fragment was placed on a support screen in the test section, and the air velocity was adjusted until the fragment rose from the screen and assumed relatively stable vertical equilibrium. This air stream velocity was then measured, and together with air density, fragment weight and average presented area, used to calculate the low subsonic drag coefficient. Air velocities for each fragment had an approximate Mach number of 0.1. Many dimensionless ratios were considered for correlation with the low subsonic Mach number drag coefficient, but the best correlation obtained was with the ratio of maximum to average presented area. To the best of my knowledge, little experimental testing of irregularly shaped fragments has been conducted beyond what is discussed above, especially in regards to supersonic speeds. Therefore, this thesis is unique in that it is the first, if not among the first, to experimentally investigate lift and drag forces on irregularly shaped fragments in the supersonic range.

1.2.2: NACA/NASA and the National Unitary Wind Tunnel Plan, 1945-1965

Since a large portion of this thesis details the design and construction of the supersonic wind tunnel used to conduct the experimental tests, the following papers presented are about the need for new supersonic wind tunnels, and the renovation/optimization of existing facilities. In 2002,Launius and Irvine (NASA), and Arrington (QSS Group Inc.) conducted a study in the interest of renewing America's investment in aeronautics research and technology, and the necessary ground test facilities. The paper discusses the history of the National Unitary Wind Tunnel Act of 1949, and reviews several studies conducted by the DoD, NASA, and other organizations on the current state of wind tunnels, and emphasizes the need to compile these studies into legislation which will ensure the nation's aeronautics capabilities. Following World War II, efforts to drive the aerospace sciences through a program of high speed and altitude, and the need to establish research facilities were conducted and identified by the National Advisory

Committee on Aeronautics (NACA) and the United States Army Air Force (USAAF). The National Unitary Wind Tunnel Act of 1949 addressed the needs identified by these agencies, along with input from the aerospace industry and various educational institutions. The Act provided funding for three new, large supersonic tunnels to be built at NACA sites, the upgrade of other NACA facilities, support of selected facilities at educational institutions, and what eventually became the Arnold Engineering Development Center (AEDC). The three NACA supersonic tunnels constructed under the Act included the Ames Aeronautical Laboratories Unitary Plan Wind Tunnel, a Unitary Plan Wind Tunnel at the Langley Aeronautics Laboratory, and a 10 ft. by 10 ft. Supersonic Wind Tunnel at the Lewis Flight Propulsion Laboratory. Prior to the construction of supersonic wind tunnels, high speed research was conducted mainly using the "falling body technique," which consisted of dropping objects from a high altitude, and by using rockets to achieve supersonic speeds. The five studies reviewed by Launius, Irvine, and Arrington identify existing facilities of significance to be maintained and utilized, as well as new facilities necessary to pursue new technologies. All of the studies reviewed discuss a need for funding in order to upgrade existing facilities, and construct new wind tunnel complexes. Launius, Irvine, and Arrington conclude that since a direct correlation has been drawn between R&D investment and excellence in technology, legislation must be enacted to ensure U.S. technological superiority.

1.2.3: Supersonic Wind Tunnel Optimization

Bushnell and Tripi (1986) conducted a study to examine the capabilities of supersonic wind tunnels at the time, specifically in regards to their application and facility related technology, in order to suggest what could be accomplished by modernizing these supersonic facilities. Due to the large number of different applications, information to be gathered, and parameters to be matched, a single facility which could meet the required capabilities would be too expensive and overloaded with work. Therefore, an assortment of facilities with different wind tunnel types and capabilities were constructed in order to meet the requirements of supersonic testing. The majority of large aerodynamic tunnels are continuous and driven by axial flow compressors or ejector drives, while many of the smaller tunnels are either of blowdown or shock-tube type. Bushnell and Tripi conclude there is a need to improve the current supersonic facilities due to the changing nature/shape, of supersonic vehicles, as well as the need for greater precision. In improving these facilities they state that it will be particularly important to eliminate sting/balance effects, have detailed flow visualization capable of simulating airframe propulsion interaction and boundary layer transition, and decrease the large amounts of energy used by the large re-circulating tunnels. To address these issues, the authors suggest the following improvements; magnetic balances to eliminate the sting support and its effects during testing, a stimulated Raman spectroscopy spectrum for detailed viscous flow field diagnostics and visualization, dynamic flow control for inlet/engine testing, more efficient diffusers to reduce energy consumption, and a new facility with laminar wall boundary layers in order to investigate supersonic boundary layer transition.

1.3: Outline

Generating uniform Mach 2 flow in a 20”x 20” wind tunnel test section is not a simple task. Prior to beginning the design process for such a tunnel, tunnel sizing must be conducted to determine whether or not adequate run times will be produced. In addition, the properties of the test gas throughout the tunnel circuit must be analyzed. This task was accomplished by creating a blowdown wind tunnel analysis model discussed in the following section. Upon completing this model, and conducting the analysis of a number of parameters on wind tunnel run time, and test section/storage tank test gas properties over time, the design of tunnel components could begin.

The mechanical design of wind tunnel components such as the settling chamber, test section, supersonic nozzles, diffuser, and exhaust were conducted using SolidWorks. The process of designing these components was very lengthy, and subject to a number of revisions. In addition, stress analysis was conducted on each of these components, using the SolidWorks stress analysis solver, in order to ensure they could withstand the operating conditions of the tunnel. Tunnel components such as the pressure control valve and silencer were also researched and selected.

Upon completion of the tunnel design process, tunnel parts and components were machined and fabricated, and the tunnel was assembled as parts were finished. Once the tunnel construction was complete, shakedown testing was conducted in order to determine whether or not the tunnel was capable of producing the desired test section Mach number. Also, a control valve program capable of opening the valve quickly and in a stable manner was developed during shakedown testing.

Once it had been determined the tunnel was capable of producing the desired test section Mach number, a flow survey was conducted in order to ensure the flow was uniform throughout the region of the test section in which a fragment will be placed. This survey was conducted by placing a Pitot tube in the test section and traversing it vertically. Once the flow survey was complete, experimental testing could begin. A three component strain gauge force balance was used to measure the aerodynamic loads on two irregularly shaped fragments of differing size and shape over an “effective” 360° pitch sweep.

The following section briefly discusses the blowdown wind tunnel analysis model. Next, the design and selection of each of the wind tunnel components is discussed in detail. Then, the wind tunnel shakedown and flow survey are discussed. Finally, the experimental results and fragment force data are presented. This thesis mainly details the design and construction of the supersonic wind tunnel since only two fragments were tested.

Chapter 2.0: Supersonic Wind Tunnel Design

Experimental testing was performed at the Techsburg Wind Tunnel Facility. In order to test at the desired Mach number of 2, as well as provide for the testing of larger models, the design of a new supersonic wind tunnel was necessary. The type of tunnel chosen to be designed was the intermittent blowdown tunnel, since they are generally simpler to design and less costly to build and operate than a continuous tunnel. Another advantage of the intermittent tunnel over other types, such as the continuous or indraft, is that model testing is more convenient since large amounts of time do not have to be spent pumping down the tunnel circuit or getting the drive motors up to speed. In addition to cost, one of the largest constraints on the design of the supersonic wind tunnel was available space, particularly in regards to component length. The entire supersonic wind tunnel had to fit in a space roughly 30 ft x 50 ft. The air storage tanks are brought up to operating pressure by a Kaeser CSD-100S screw type compressor, rated to 217 psig with a 288 cfm capacity. Since the only existing hardware at the experimental test facility consisted of two horizontal air storage tanks, wind tunnel components such as the settling chamber, test section, supersonic nozzles, diffuser, and exhaust had to be designed. In addition, the selection of a control valve, silencer, and additional air storage tanks was necessary. However, before beginning the process of designing and selecting wind tunnel components, an analysis model was created in order to predict the flow properties of the test gas throughout the wind tunnel circuit. This spreadsheet is briefly discussed in the following paragraph. Next, the design of each of the wind tunnel components is presented.

2.1: Blowdown Wind Tunnel Analysis Model

In order to determine the properties of the test gas throughout the wind tunnel circuit, as well as analyze the effects of a number of variables on wind tunnel efficiency and run time, a supersonic blowdown wind tunnel analysis model was created. The variables which the user can input into the model include the following: air storage tank volume and total pressure, polytropic expansion coefficient, diffuser pressure recovery, ambient temperature and pressure, test section cross-sectional area, test section Mach number, and silencer pressure loss. In addition, pressure losses from the air storage tanks to the control valve through the pipe immediately downstream of the valve are included, allowing for a more accurate representation of the percent of air in the storage tanks vs. time. The implementation of this model displayed the influence of a number of variables on wind tunnel run time, and provided values used in stress analysis calculations. The methods and equations used in the analysis model are discussed in detail in Appendix A.

2.2: Air Storage Tanks

Based on information obtained from the blowdown analysis spreadsheet, it was determined that additional air storage tanks were required in order to produce adequate wind tunnel run times. Two 1,550 gallon vertical air receivers were added to the wind tunnel facility, increasing the total storage capacity to 10,700 gallons. Vertical air receivers were chosen in

order to maximize the allowable floor space of the wind tunnel room. Custom flanges were added in order to allow the receivers to mate up with each other and the existing storage tanks. The air storage tanks can be seen below in Figure 2.1.

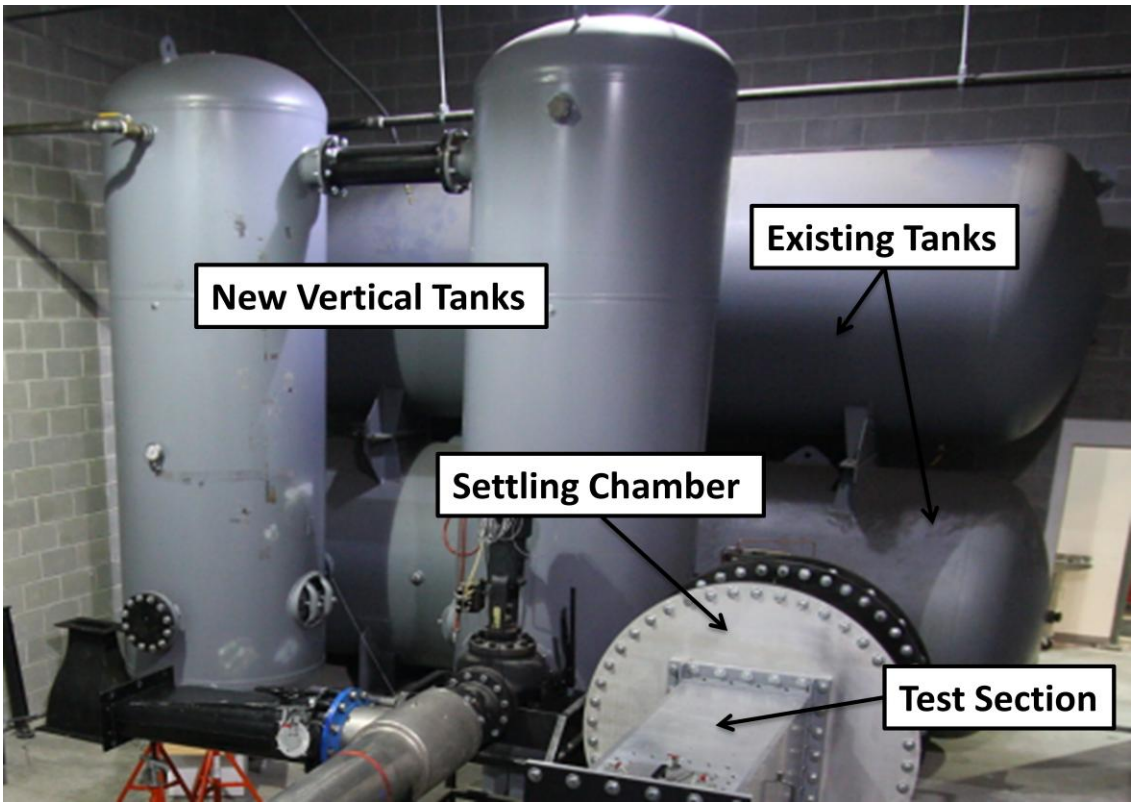

Figure 2.1. Wind tunnel facility compressed air storage tanks, total storage capacity of 10,700 gallons. The settling chamber and test section can be seen in the lower right hand corner.

2.3: Control Valve

The blowdown wind tunnel is designed to operate at a constant stagnation pressure during runs. The control valve maintains a constant wind tunnel stagnation pressure as the available pressure in the storage tank decreases. A new control valve was necessary in order to handle the high mass flow rates, approximately 240 lbm/s, associated with supersonic flow through a 20" test section. After conducting extensive research, a 12" Fisher Vee-Ball Control Valve was selected. A photo of the control valve can be seen below in Figure 2.2. The V-notch ball in this control valve provides an approximately equal percentage flow characteristic, meaning that equal increments of valve travel produce equal percentage changes in the existing flow, increasing accuracy for the control of the wind tunnel. The ball in the control valve also contains an attenuated section in order to decrease the noise resulting from the air flowing through the valve. Also, volume boosters are installed on the valve in order to allow it to open and close very quickly. During wind tunnel shakedown a significant amount of effort was required to define the values in the control valve program which would allow the valve to open

in a stable manner, generate Mach 2 flow in the test section, and close as quickly as possible. Also, in order for the valve to open and close as quickly as possible, the optimum opening of the needle valves in the volume boosters had to be determined. The valve position is controlled by a Siemens Moore 353 Process Automation Controller, and incorporates an emergency shutoff switch that closes the valve should something catastrophic occur.

Figure 2.2. Fisher 12" Vee-Ball Control Valve and inlet pipe to supersonic wind tunnel wide angle diffuser. The valve components and copper tubing attached to the body are the volume boosters, and safety trip valve.

2.4: Settling Chamber

In order to improve the flow uniformity in the wind tunnel, a large area low velocity section is placed immediately upstream of the nozzle. This section produces a large contraction of the flow as it enters the nozzle, and is generally referred to as the settling chamber. The transition to this larger area section is accomplished by a wide angle diffuser, which increases from the 12"diameter inlet pipe to 48" in diameter at a double wall angle of approximately 40 degrees. An image of the settling chamber and wide angle diffuser can be seen below in Figure 2.3. Relatively long low angle diffusers have been tried, but Pope states that the most common angles between opposite walls include those ranging from 45 to 90 degrees. In order to break up the highly turbulent and non-uniform flow exiting the control valve, a pyramid shaped flow

spreader is installed within the wide angle diffuser. The flow spreader consists of four, perforated, 0.25 inch thick sheet metal equilateral triangles welded to a flange in the shape of a pyramid. The open area ratio of the flow spreader is approximately 53%, and is bolted in between the wide angle diffuser and settling chamber. The settling chamber is a cylindrical shell, one diameter in length, which Pope states is the required minimum length to obtain uniform flow. A honeycomb structure is located at the entrance of the settling chamber, and forces the flow over the entire cross sectional area of the settling chamber to be moving in the same direction. The honeycomb is 51" in diameter, with a ¼" cell size and length to diameter ratio of 6.

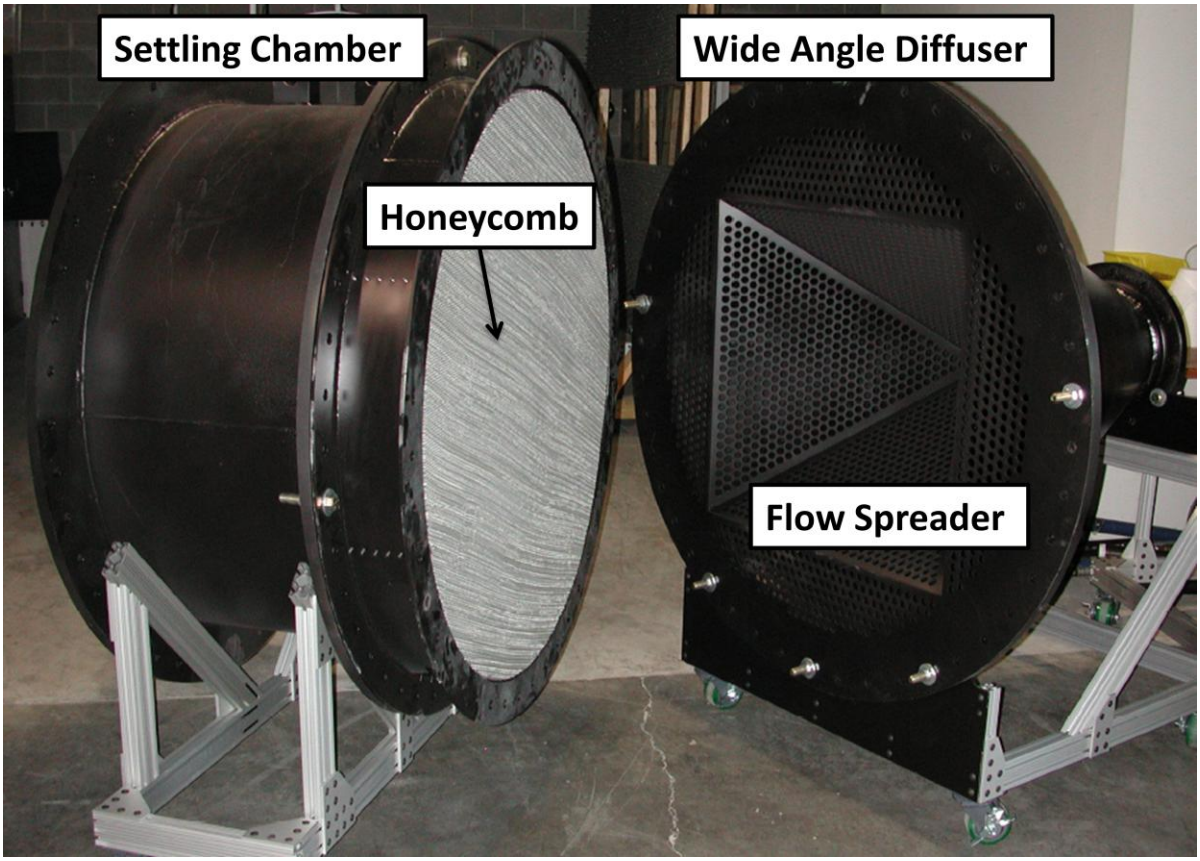

Figure 2.3. The settling chamber (on the left) and wide angle diffuser (on the right) can be seen disassembled above. The pyramid shaped flow spreader and honeycomb structure can be seen in this orientation.

In addition, a screen is located downstream of the honeycomb in order to further promote flow uniformity. These screens produce a resistance to the flow, equivalent to the pressure drop through each screen, and can be determined from the expression shown below in Equation 2.1 (Schubauer, 1950).

$$p_2 - p_1 = \frac{1}{2} K \rho V^2 \qquad \textbf{Equation 2.1}$$

Where, K is the screen pressure drop coefficient, and is dependent on Reynolds number and the ratio of area blocked by the wires of the screen to total duct area. The screens used have a wire diameter of 0.009" and an open area ratio of approximately 67%. Using the plot shown below in Figure 2.4 (Pope, 1965), K is found to be about 0.37, and along with flow density and velocity in the settling chamber, the pressure drop through a single screen is determined to be around 0.3 psi.

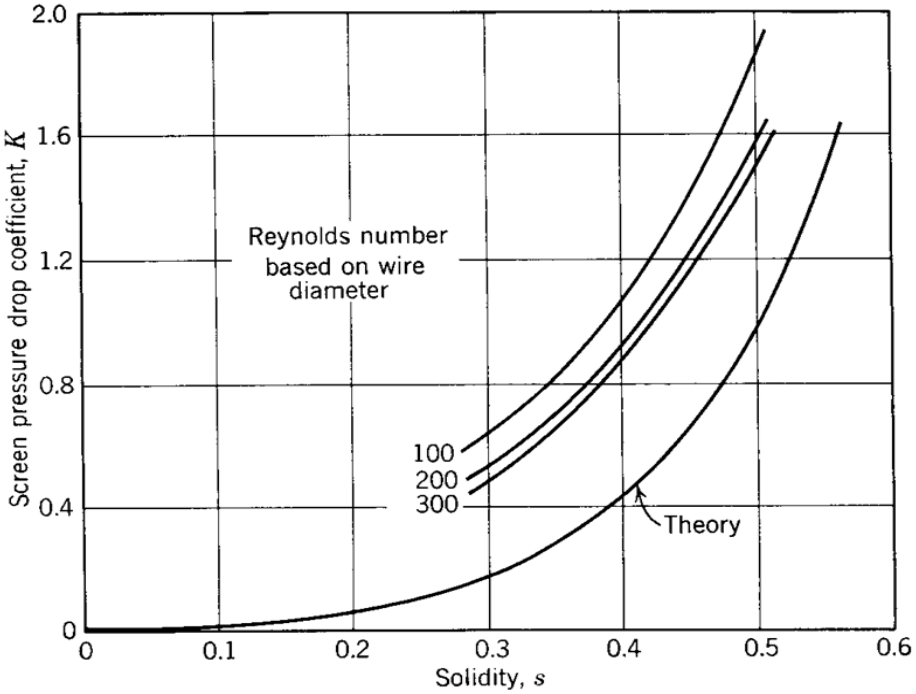

Figure 2.4. Pressure drop through screens. (Plot obtained from High Speed Wind Tunnel Testing, Pope 1965).

At the end of the settling chamber is a 59.5" diameter blind flange, which has a square cutout that the sub-sonic portion of the nozzle and test section fit into. A bellmouth is bolted to the outer walls of the test section in order to provide smooth transition of the flow from the settling chamber to the subsonic portion of the nozzle and into the test section. A picture of the bellmouth can be seen below in Figure 2.5. This bellmouth consists of a top, bottom, and side transitions pieces that form a sort of picture frame that fits around the portion of the test section that extends into the settling chamber. The top and bottom bellmouth pieces match the angle of the subsonic portion of the nozzle. Angle plates are bolted to the walls of the test section and the blind flange in order to keep the test section in place as tremendous thrust loads are placed on it during wind tunnel runs.

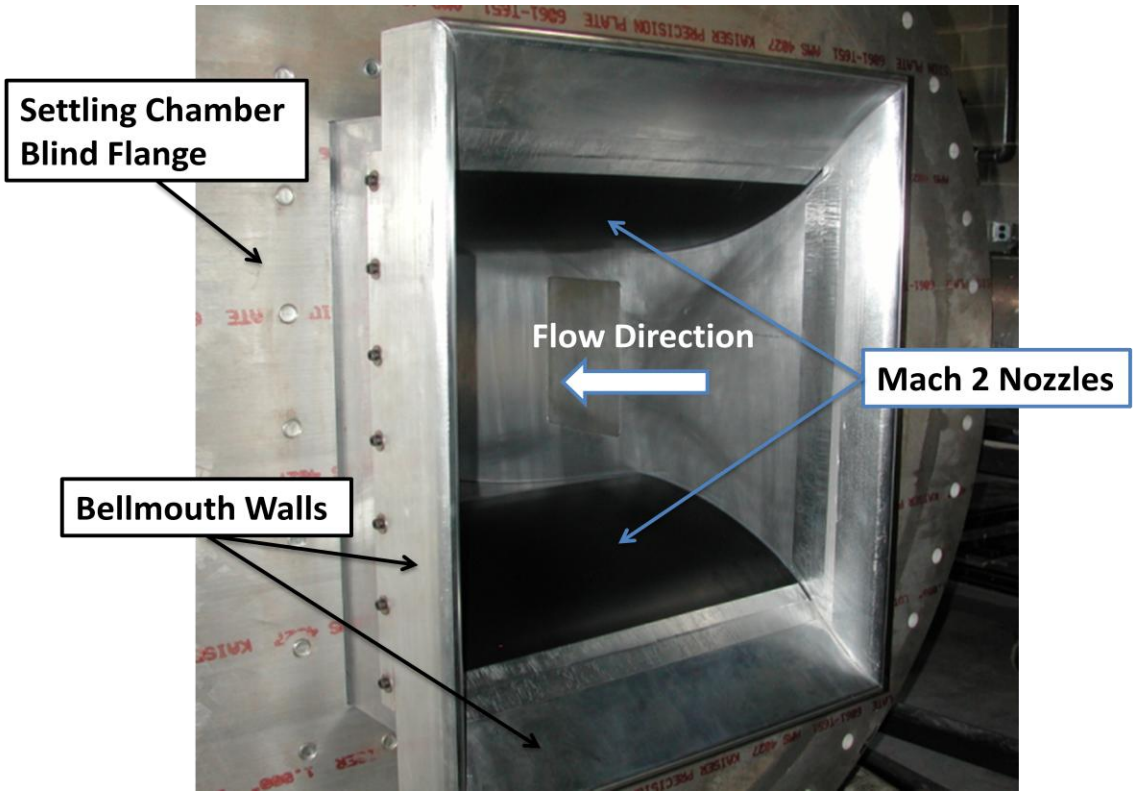

Figure 2.5. Bellmouth which helps to smoothly transmit flow from the settling chamber into the subsonic portion of the nozzle and test section. The large diameter blind flange which bolts to the end of the settling chamber and connects the test section to the settling chamber can be seen in the background.

2.5: Nozzles

In order to test at the desired Mach number of 2, a supersonic nozzle had to be designed and fabricated. A method of characteristics code was used in order to determine the contours of the diverging section of the nozzle. In using this method the diverging portion of the nozzle is divided into a series of straight sections in order to define the characteristic lines and their respective reflections and cancellations. Inputs for the code include test section Mach number, height, and length, number of characteristics, and a parameter to control the wall curvature. The rule of thumb for the number of characteristics is considered to be approximately six times the test section Mach number, and controls the initial wall turning angle. The output of the code is a series of points in the x-y plane which represents a contour of the diverging section of the nozzle that will produce a uniform Mach number in the test section. CFD was performed by Techsburg in order to validate the design of the nozzles, as well as the rest of the tunnel flow path. This CFD simulation is discussed below in Section 2.7, and a contour plot of Mach number throughout the tunnel flow path can be seen in Figure 2.12. The nozzles were fabricated from sheet metal that was rolled and formed to match the contours output by the method of characteristics code. An image of the Mach 2 nozzles can be seen in Figure 2.6 below.

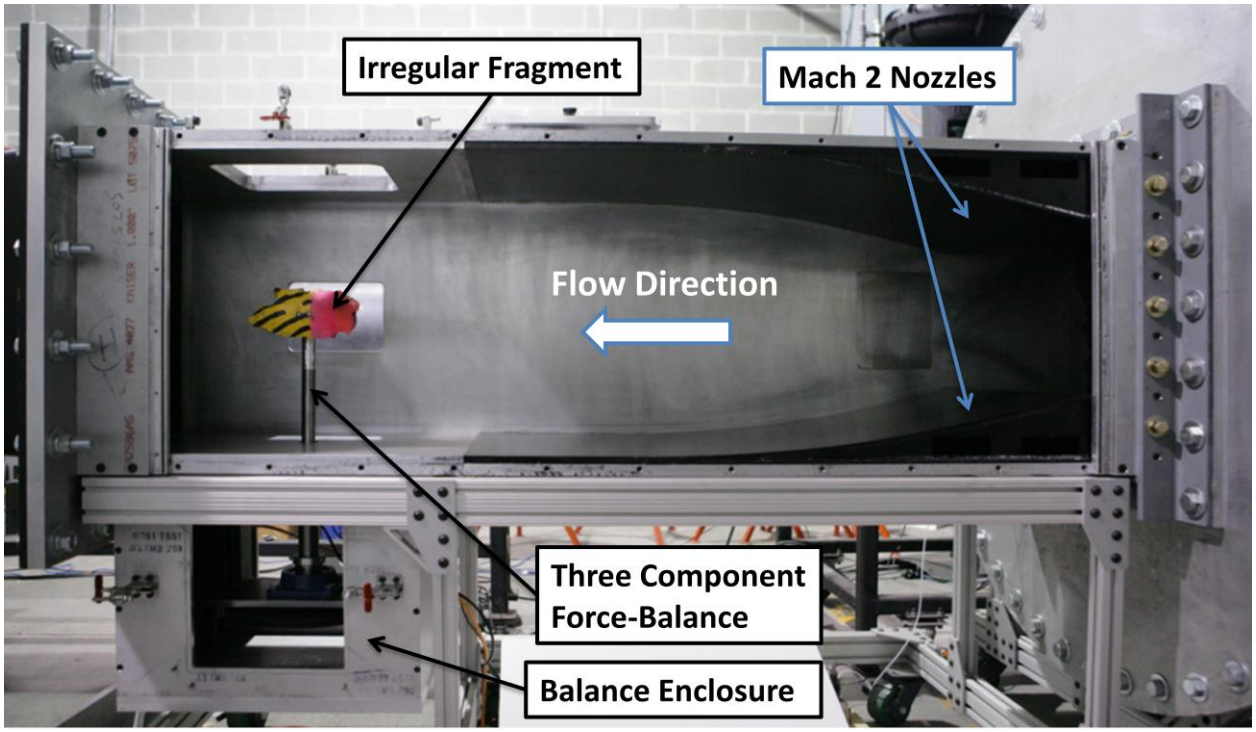

Figure 2.6. With the test section side wall removed, the Mach 2 nozzles can be seen above. The subsonic portion of the nozzles and bellmouth extend into the settling chamber. The angle plates which attach the test section to the settling chamber can also be seen.

2.6: Test Section and Balance Enclosure

One of the largest considerations in the design of a supersonic wind tunnel is the size of the test section. In addition to constraining the size of models capable of being tested, the cross sectional area of the test section has a large influence on tunnel mass flow rate and run time. In regards to allowable model size, two primary considerations are to ensure that reflected shocks do not impinge on the model, and that model blockage is not too great as to prevent the tunnel from attaining its designed test section Mach number. Based on values obtained from the blowdown analysis model and CFD simulations, it was decided that the cross sectional area of the test section would be 20" x 20". Although an exact procedure for determining allowable model length does not exist, upon making a few approximations, reasonable estimates can be made for maximum model length using Equation 2.2 below (Pope, 1965). Where, θ is the shock wave angle, μ is the angle of the shock reflection, and α is the model angle of attack. An image of shock waves coming off a test section model, and their reflections can be seen below in Figure 2.7 (Pope, 1965).

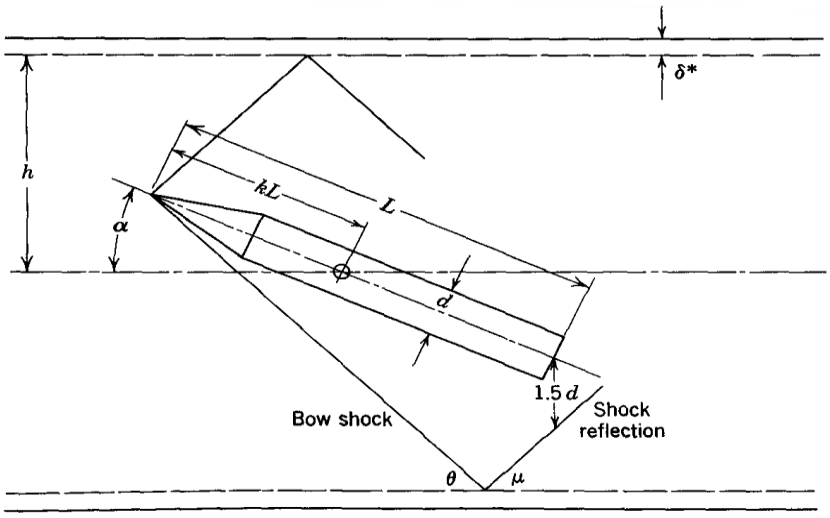

Figure 2.7. Example of bow shock on a model placed in a test section, and the shock reflection off the test section wall. (Figure obtained from High Speed Wind Tunnel Testing, Pope 1965)

$$L_{max} = \frac{h(1+\tan\mu\cot\theta)}{1.5/(L/d)+\cos\alpha\tan\mu} \qquad \textbf{Equation 2.2}$$

The allowable model size for a given test section area and Mach number can be determined using the plot shown below in Figure 2.8 (Schueler, 1960). From this plot, with a test section cross sectional area of 400 in^2 and Mach number of 2, the maximum testable model size is approximately 38 in^2. The supersonic test section can be seen below in Figure 2.9.

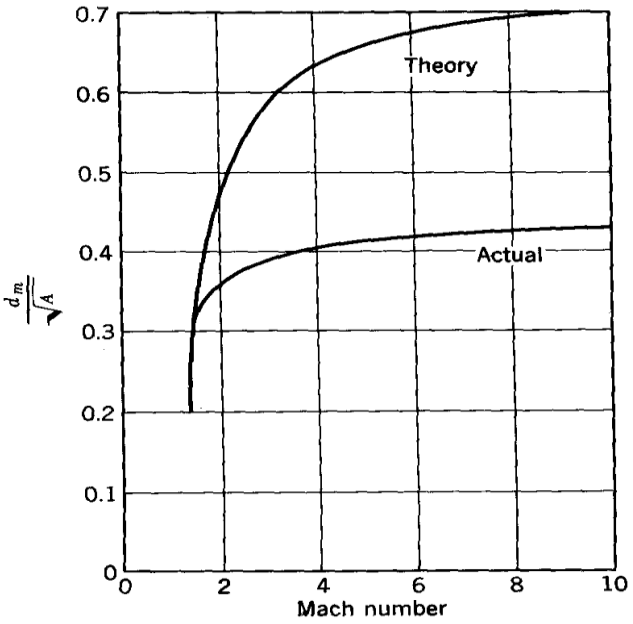

Figure 2.8. Plot of maximum model diameter, d_m, that will allow the tunnel to be "started" for a given test section size and Mach number. (Plot obtained from An Investigation of Model Blockage for Wind Tunnels at Mach Numbers 1.5 to 19.5, Schueler 1960).

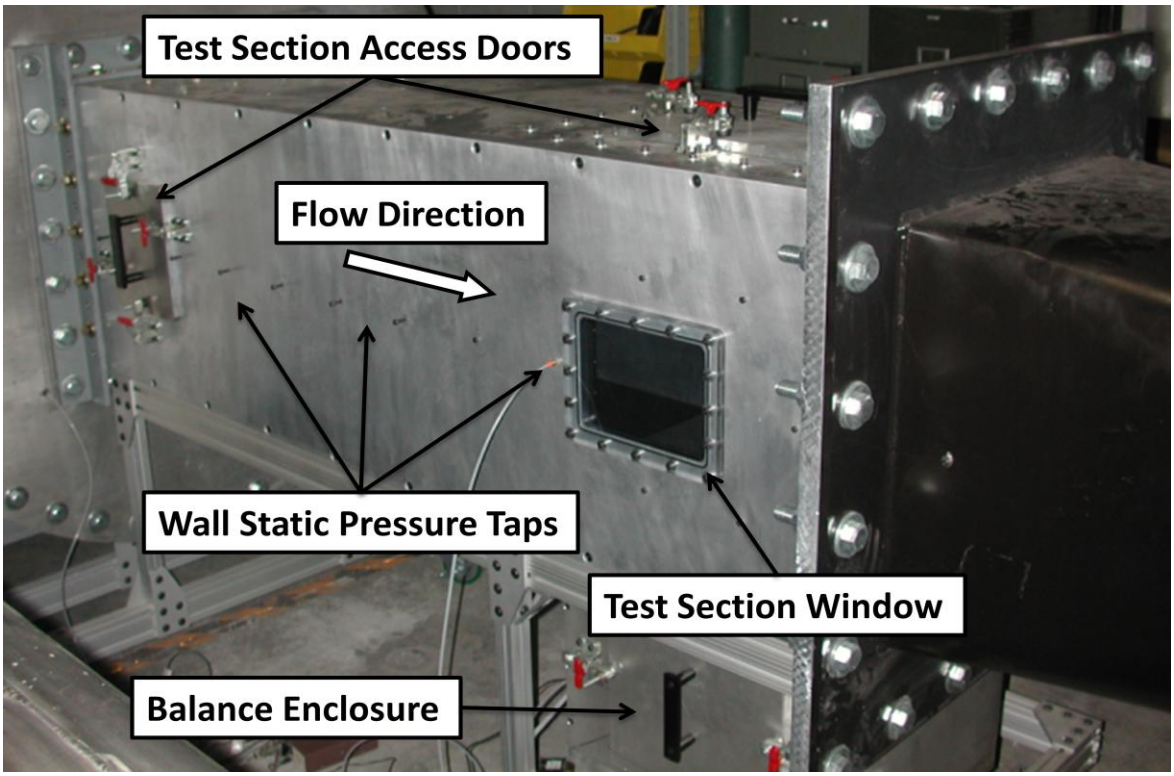

Figure 2.9. 20" x 20" supersonic wind tunnel test section. Test section access doors, window, and wall pressure taps can be seen.

The balance enclosure houses the force balance support shaft, and turntable drivetrain and stepper motor used to vary the fragment's orientation with respect to flow direction. The motor used is an Intelligent Motion Systems integrated stepper motor. The motor has a 1.5 in. pinion gear that drives a 12 in. diameter spur gear, resulting in an 8:1 gear ratio. The 12 in. spur gear is mounted on the 1.5 in. support shaft, which the three component force balance attaches to. The support shaft is held in place by a large radial bearing and shaft collar, and the force balance is supported by a radial bearing in the floor of the test section. The balance enclosure can be seen below in Figure 2.10.

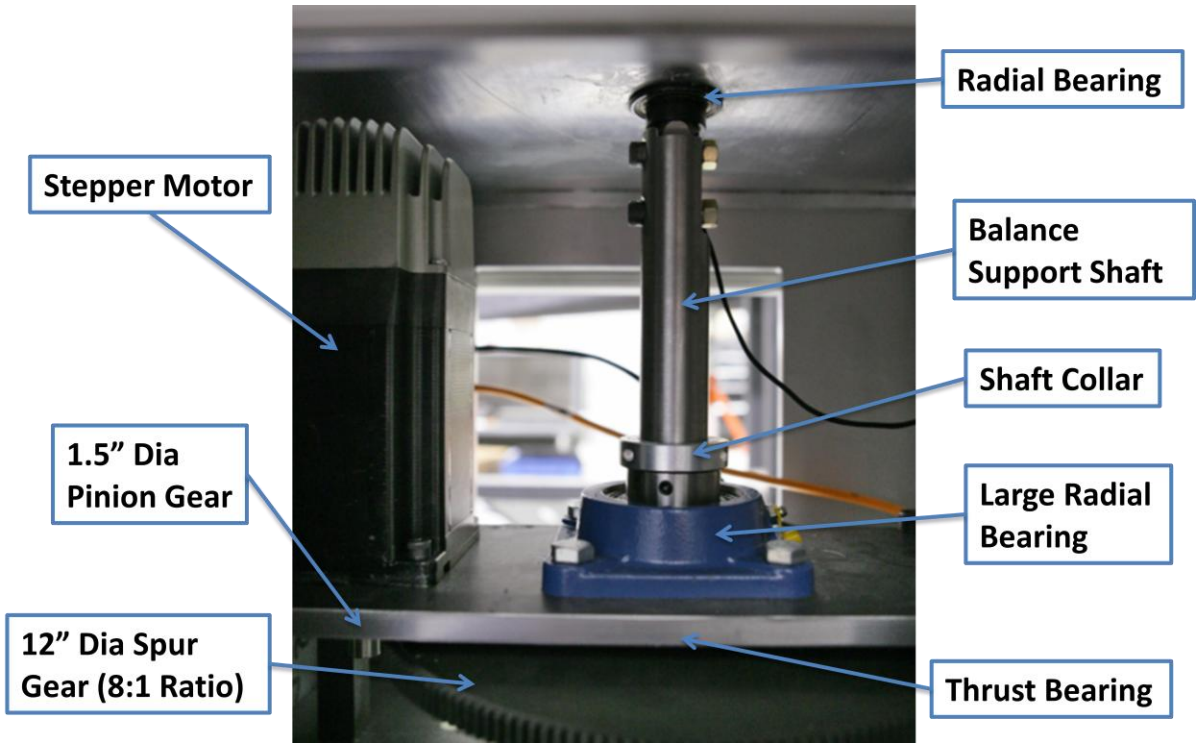

Figure 2.10. Wind tunnel balance enclosure with stepper motor and gear drivetrain used to vary balance pitch angle. In addition the support shaft, radial bearings and shaft collar used to constrain the force balance to rotational motion only can be seen.

2.7: Diffuser

In order to recover the pressure head of the flow, a diffuser is installed immediately downstream of the test section. To decrease the speed of the flow in a supersonic wind tunnel, a shockwave is generally used, however when a supersonic flow passes through a shock wave, a loss in total pressure occurs. This loss in total pressure contributes significantly to the power requirements of supersonic tunnels. It has been proven that the total pressure loss associated with decelerating a flow to subsonic speeds through a normal shock at the test section Mach number is much greater than if the normal shock were to occur at a lower Mach number, ideally unity. This fact has led to most diffusers being designed with a converging section, minimum area diffuser throat, and diverging section. Within the converging section of the diffuser the flow is compressed and decelerated to a Mach number lower than that in the test section. After passing through the diffuser throat the flow will accelerate slightly as the area increases in the diverging section until a normal shock is established at a Mach number lower than that of the test section, with an accompanying reduction in total pressure loss. However, it has also been shown that diffuser throat sizes capable of "starting" a tunnel are considerably larger than that needed for the diffuser throat to be around Mach 1 during operation. Therefore, it is concluded that if the diffuser throat could be opened to an area capable of "starting" the tunnel, and then closed to a more optimum area ratio after the shock has passed through the throat, the pressure ratio requirements of running the wind tunnel will be significantly reduced. Since diffuser

performance has such a large influence on tunnel sizing and run time, variable throat diffusers were investigated in an attempt to achieve the highest possible pressure recovery.

In early 1950, tests were conducted at the U.S. Naval Ordnance Laboratory in order to determine the most efficient diffuser configuration for use in a supersonic wind tunnel (Diggins, NAVORD Report). From these tests it was determined that a converging-diverging diffuser with a variable throat located at 42% the overall diffuser length resulted in the best pressure recovery. In addition, a throat located at 20% achieved similar, but slightly lower, pressure recoveries. However, this optimum pressure recovery is obtained at some throat opening not able to start the tunnel. Therefore, the diffuser throat must begin at some larger value until supersonic flow is established, upon which the diffuser throat can be closed to the optimum value, resulting in a large increase in pressure recovery and wind tunnel run time. With optimum diffuser throat location and area ratio, Diggins observed pressure recoveries of approximately 1.35. It must be noted that Diggins defines this pressure recovery as the measured diffuser pressure ratio divided by the pressure ratio associated with a normal shock at the test section Mach number. This definition differs from the standard definition of pressure recovery coefficient found in most textbooks, and shown below in Equation 2.3 (White, 1994). Therefore, by Diggins' definition, a diffuser with a pressure recovery of 1.35 is 35% more efficient than a simple fixed converging diffuser which decelerates the flow to subsonic speeds through a normal shock at the test section Mach number.

$$C_p = \frac{p_2 - p_1}{p_{01} - p_1} \qquad \textbf{Equation 2.3}$$

Many different variable throat diffuser designs were investigated, however due to cost constraints and the increased complexity associated with a variable throat diffuser, a fixed throat converging-diverging diffuser was chosen. In addition to increased cost and complexity, it is often the case that variable throat diffusers do not perform as well as expected. Even though the Diggins NAVORD Report stated optimum pressure recovery occurred with a diffuser throat located at 42% of the overall diffuser length, due to space constraints in Techsburg's facility, the final location of the throat in the fixed converging-diverging diffuser was chosen to be at 20% the overall length. This throat location demonstrated only slightly lower pressure recoveries than 42%, and the increased length of the diverging section allows for greater subsonic diffusion. The cross sectional area of the diffuser throat which will allow the normal shock to pass through during the starting process is determined using Equation 2.4 below for Mach 2 flow (Pope, pg. 32). Using this equation the diffuser throat diameter was determined to be 20.46".

$$\frac{A_2^*}{A_{TS}} = \frac{\left(5 + M_{TS}^2\right)^{0.5}\left(7M_{TS}^2 - 1\right)^{2.5}}{216M_{TS}^6} \qquad \textbf{Equation 2.4}$$

The assumptions associated with this equation are that the Mach number in the second throat is 1, and the expansion of the air from the conditions downstream of the normal shock in

the test section to Mach 1 at the diffuser throat is an isentropic process. Since the test section is square, and the silencer inlet round, a transition piece is necessary, and is implemented in the converging section of the diffuser. Upon passing through the diffuser throat, subsonic diffusion is accomplished through the conically shaped diverging section. Since the inlet diameter of the silencer is 30.25", after determining the diffuser throat area using the equation above, the area ratio and angle of divergence of the subsonic diverging section become fixed. The length of the diverging section is also dependent on the allowable space in between the converging section and silencer inlet. An image of the fixed throat converging-diverging diffuser can be seen in Figure 2.11 below. The area ratio of the conical subsonic diffuser is 2.19 and the ratio of diffuser length to inlet radius is 11.73. Based on a conical performance diffuser map from (Ishikawa and Nakamura, Diff Design Tech), a pressure recovery coefficient, C_p, of approximately 0.75 can be expected in the diverging section of the diffuser.

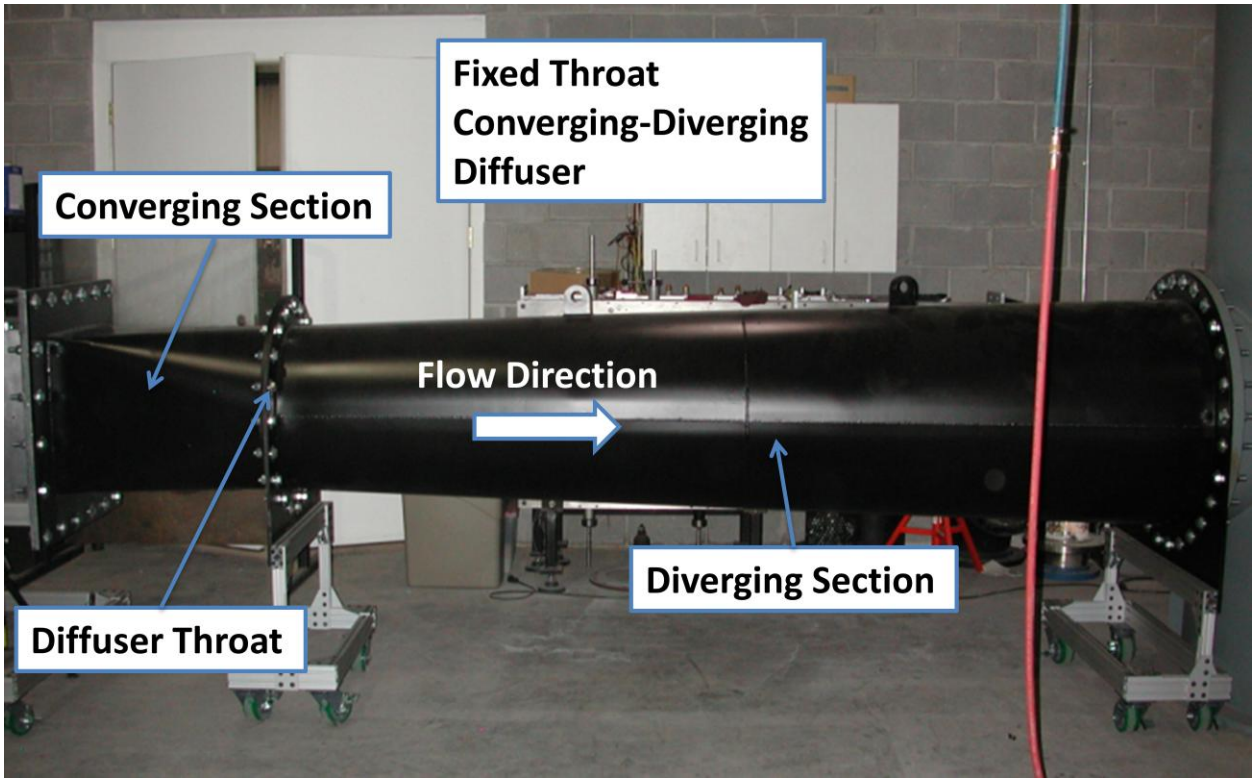

Figure 2.11. Supersonic wind tunnel fixed throat, converging-diverging diffuser.

In order to analyze diffuser performance, computational fluid dynamics (CFD) simulations of the nozzle/test section/diffuser assembly were performed by Techsburg. Viscous, 3-D simulations were conducted on a quadrant of the tunnel flow path, with the Mach 2 nozzle designed using the method of characteristics code discussed earlier, and the fixed throat converging-diverging diffuser geometry. A contour plot of Mach number throughout the simulated tunnel circuit can be seen below in Figure 2.12. From the plot one can see that uniform Mach 2 flow is established in the test section. Upon entering the converging section of

the diffuser (square to round transition piece) an oblique shock structure is generated and the flow decelerates slightly as the area decreases. After passing through the diffuser throat the flow accelerates as the area increases, and the oblique shock structure continues until a normal shock is generated. Around the location of this normal shock it can be seen that the flow has separated and is highly variable and erratic downstream of the shock. This flow separation reduces the performance of the diffuser, and contributes to the overall pressure losses of the tunnel circuit, decreasing run time. The diffuser pressure recovery from this simulation, as defined by Diggins, was determined to be 0.94 ± 0.19 with 95% confidence. The large uncertainty in this value is mainly due to the highly variant and erratic flow structure exiting the diffuser.

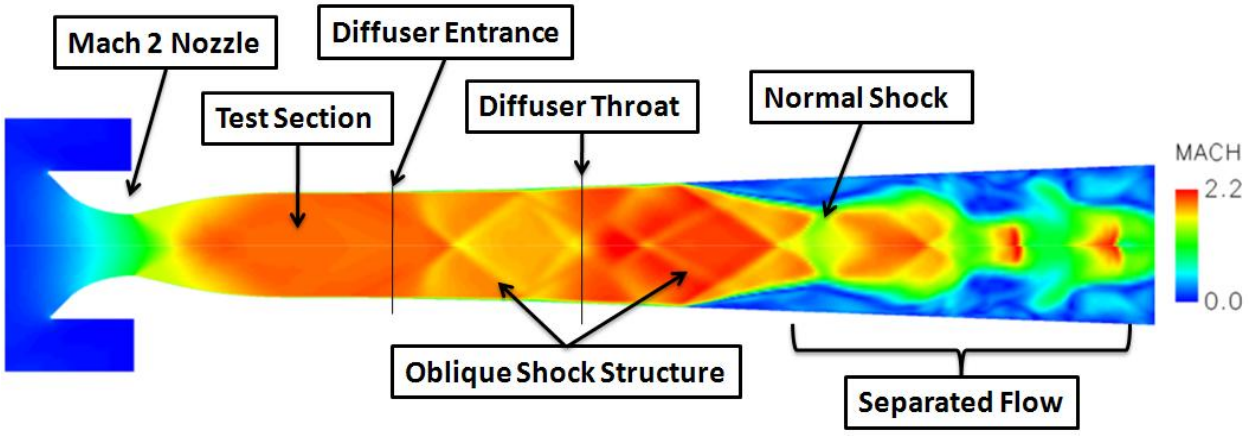

Figure 2.12. Contour plot of Mach number from CFD simulation of nozzle/test section/diffuser assembly.

2.8: Silencer

The noise output from a supersonic wind tunnel can be harmful at short distances and very annoying at large ones. Therefore, a silencer is required downstream of the diffuser in order to muffle this noise. The silencer selected for the supersonic wind tunnel was the Burgess-Manning SDA-44-2 Silencer, and was the largest industrial, side-inlet silencer capable of fitting in the wind tunnel room. An image of the silencer can be seen below in Figure 2.13. The silencer has a 30" diameter horizontal inlet pipe, a 56" diameter body, and a 30" diameter outlet. The inlet of the silencer contains a perforated cylindrical pipe that protects the acoustic treatment material from the high velocity air stream exiting the diffuser. Also, the perforated pipe provides controlled pressure expansion to atmosphere, as well as a shift of low frequency noise to the more easily attenuated high frequency bands. Within the body of the silencer are a number of concentric cylinders packed with acoustic dampening mineral wool. Utilizing a pressure tap in the wall of the diffuser near the silencer inlet, it was determined that the silencer total pressure loss is approximately 18 psi. This large pressure loss reduces the efficiency of the tunnel, and results in higher mass flow rates, and decreased tunnel run time. However, since the noise levels produced by supersonic wind tunnels are so high, the silencer is a necessary component for operation.

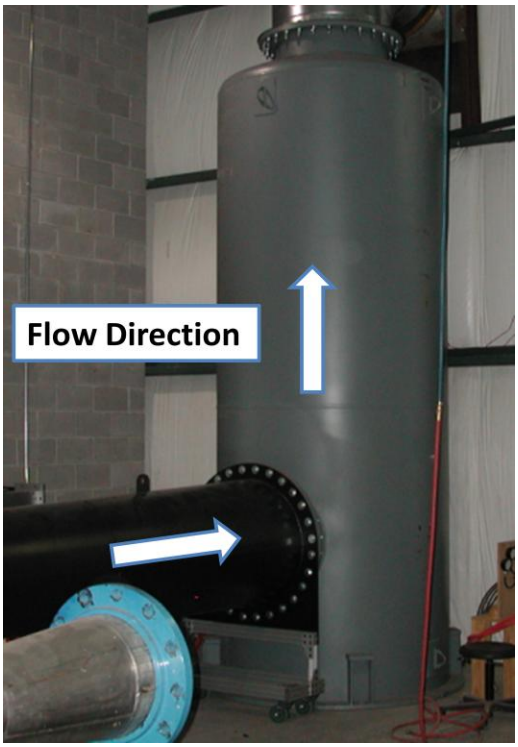

Figure 2.13. Supersonic wind tunnel silencer.

2.9: Exhaust

In order to vent the air from the wind tunnel to atmosphere, an exhaust stack is located downstream of the silencer. In addition to allowing the air to exit the tunnel circuit and vent to atmosphere, the exhaust must also prevent water and debris from entering the wind tunnel. Allowing water to enter the exhaust and silencer would cause the absorptive material in the silencer to deteriorate and decrease its efficiency. Due to the very high mass flow rate of the supersonic tunnel, a custom exhaust was designed and fabricated from 0.25" thick sheet metal. Pictures of the tunnel exhaust can be seen below in Figures 2.14 and 2.15. Air exiting the silencer is exhausted straight up through the roof of the facility, creating for a safe downward load path. The exhaust consists of a long 30" diameter inner pipe that mates with the silencer exit flange, and a shroud pipe 42" in diameter at its exit in order to further decrease noise. The momentum of the exiting air produces a large drag force of approximately 4500 lbf on the shroud pipe. Therefore, the shroud pipe is welded and attached to the inner pipe using eight I-beams. In addition, steel angle is welded to the outside of the shroud pipe in order to increase its stiffness. Lastly, the exhaust employs rain flaps, held in place by corrosion resistant bearings, that prevent water and debris from entering the tunnel, and open under pressure during experimental runs.

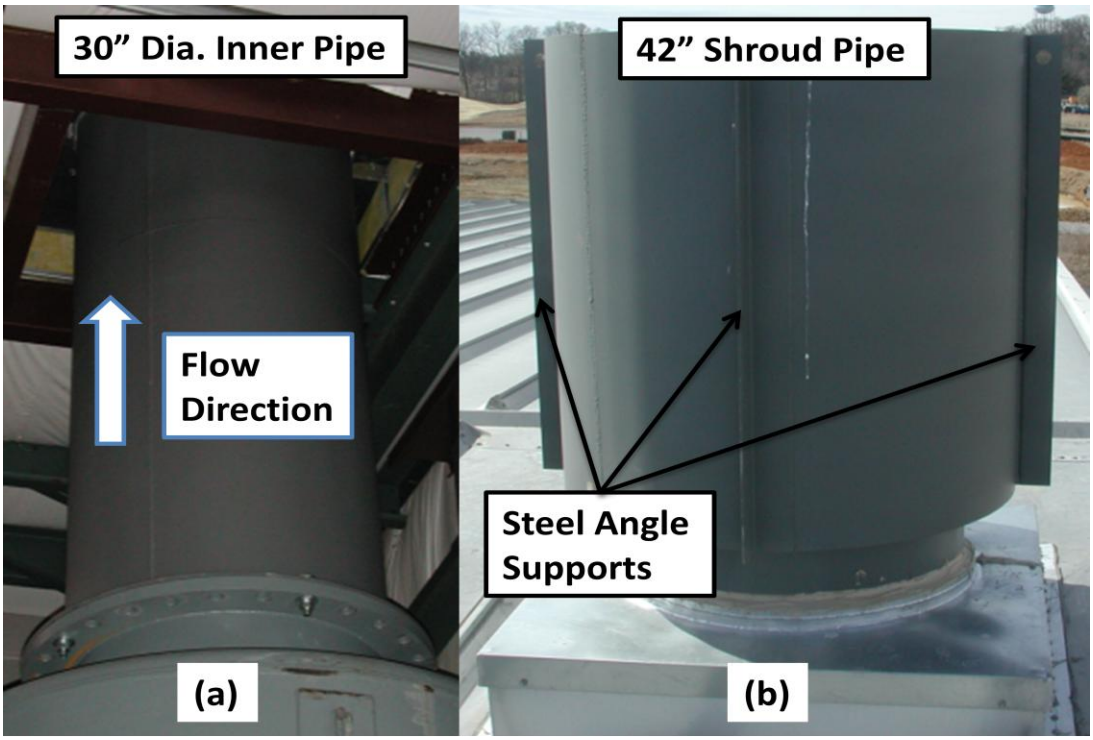

Figure 2.14. (a) 30” diameter inner exhaust pipe exiting through facility roof. (b) 42” diameter shroud pipe on top of facility roof, steel angle supports welded to shroud pipe can be seen.

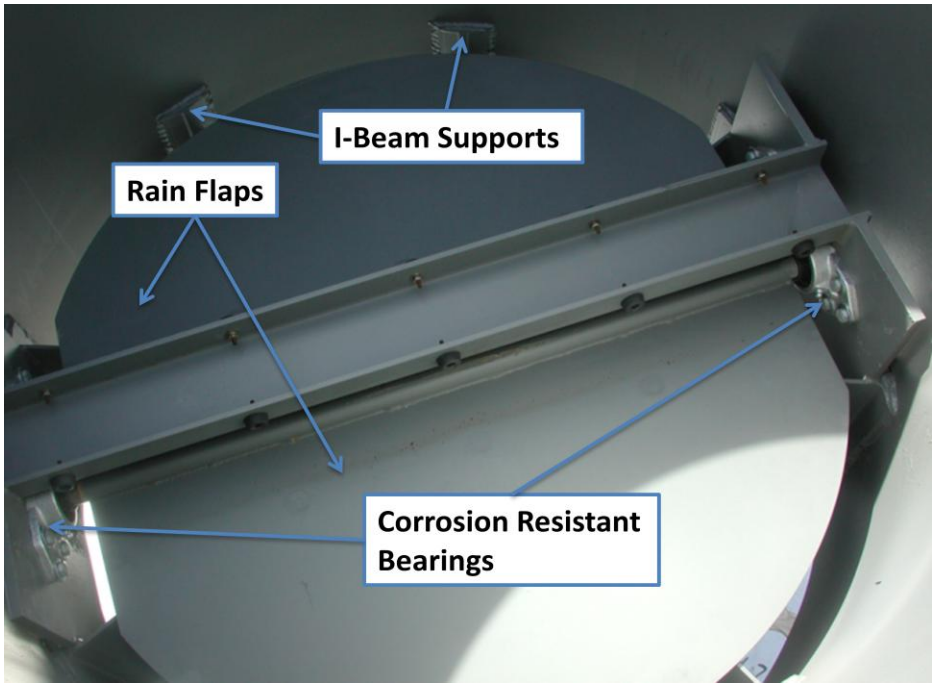

Figure 2.15. Picture of exhaust rain flap assembly, as seen looking down into exhaust from above the shroud pipe.

Chapter 3.0: Instrumentation and Data Acquisition

3.1: Pressure Measurements

In order to determine the properties of the flow and Mach number at different locations along the tunnel flow path, a number of wall static pressure measurements were taken. The stagnation temperature and pressure in the compressed air storage tanks were measured using a k-type thermocouple and pressure transducer. The absolute atmospheric pressure was also measured, since all other pressure measurements were gage values. The stagnation pressure in the tunnel was measured by means of a wall static tap and pressure transducer located in the settling chamber. Even though wall taps are used to measure static pressure, the relatively low speed flow in the settling chamber results in the static and stagnation pressures being approximately equal. Static pressure taps are located along the entire length of the nozzle, test section, and diffuser. With knowledge of the tunnel stagnation pressure, these static pressure taps allow the Mach number, and shock placement/location, along the entire tunnel circuit to be determined. For instance, static pressure taps along the length of the supersonic nozzle and test section, seen in Figure 2.6, are used to determine if and when/where the desired test Mach number has been established. This is accomplished by using the isentropic, Mach number pressure relation shown in Equation 3.1.

$$\frac{p_0}{p} = \left(1 + \frac{(\gamma-1)}{2} M^2\right)^{\frac{\gamma-1}{\gamma}} \qquad \textbf{Equation 3.1}$$

3.2: Force Balance Measurements

In order to measure the forces on the fragment in the test section, a three component strain gage force balance is used. The balance has three force channels oriented along its principal axes, each with a 1000 lbf capacity, that measure the aerodynamic loads on the model during testing. The force balance can be seen below in Figure 3.1 with strain gages and wiring exposed. During testing a shroud protects the strain gages, as well as prevents the measurement of the forces on the strain gages themselves instead of the forces on the model. The balance is mounted to a support shaft in the balance enclosure located below the test section, as seen in Figure 2.10.

Figure 3.1. Three component strain gage force balance used to measure aerodynamic forces during wind tunnel testing.

In order to amplify the signal coming from the strain gages on the force balance, a custom amplifier box employing Futek CSG105 strain gage amplifiers was designed. However, due to high amplitude, low frequency (1-2 Hz) electrical noise contamination between the amplifiers and the data acquisition hardware, as well as unreliable wiring connections, Techsburg's existing National Instruments SCXI-1520 strain gage amplifier was used instead. The two amplifier systems can be seen below in Figure 3.2.

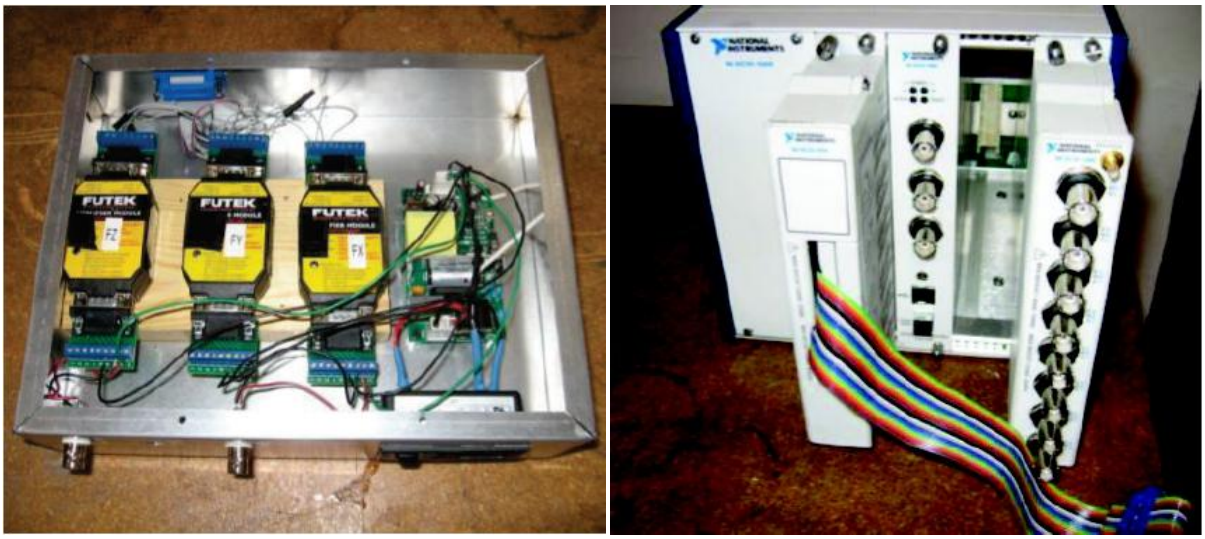

Figure 3.2. Custom strain gage amplifier box (on left), and National Instruments SCXI-1520 strain gage amplifier (on right) used to amplify and acquire the signals coming from the force balance.

Chapter 4.0: Experimental Testing

4.1: Wind Tunnel Shakedown

Upon completing the assembly of the supersonic wind tunnel, shakedown testing was conducted in order to determine if the desired test section Mach number could be produced. The supply pressure and valve opening were slowly increased, with safety in mind, until test section Mach number reached the desired value. Also during this process, after much trial and error, a valve program capable of opening the control valve in a quick and stable manner was determined. The designed valve program controls the position of the ball valve in the following manner. At the start of a wind tunnel run, the valve is opened very quickly, moving from fully closed to fully open in approximately 1 second. When the valve has reached its fully open position, Mach 2 flow is generated in the test section for approximately 0.5 seconds, after which the valve is closed as quickly as possible, in about 0.25 seconds. Therefore, the total run time for an experimental run is approximately 2-2.5 seconds. Since this run time is so short, fragments cannot be dynamically pitched during runs. Therefore, individual wind tunnel runs must be performed for each fragment orientation to be tested. However, an advantage to the short run time is that only a small fraction of the air in the storage tanks is lost, decreasing the time needed to bring the storage tanks back up to operating pressure. Following a run, the storage tanks can be brought up to pressure in approximately 15 minutes, allowing for many runs to be performed in a single day.

4.2: Flow Survey

Before conducting experimental tests a flow survey was conducted in order to ensure the flow was uniform throughout the test section, and of correct Mach number. A Pitot tube was placed in the flow through a port in the bottom of the test section and traversed through the region the models will occupy. A plot of the test section Mach number vs. percent test section height, and an image showing the Pitot probe within the test section can be seen below in Figures 4.1 and 4.2. The static pressure was measured from a wall tap in the test section, and by assuming a normal shock resided upstream of the port on the Pitot tube, the stagnation pressure measurement was numerically corrected. The Mach number at each probe height in the test section was then calculated using the isentropic Mach number pressure relation. The flow survey indicated that within the middle 60% of the test section, the average Mach number was 1.950, and varied by only 0.56% within this region. So, even though the wind tunnel run time is short, the Mach number uniformity during the window in which the test section remains started is very good.

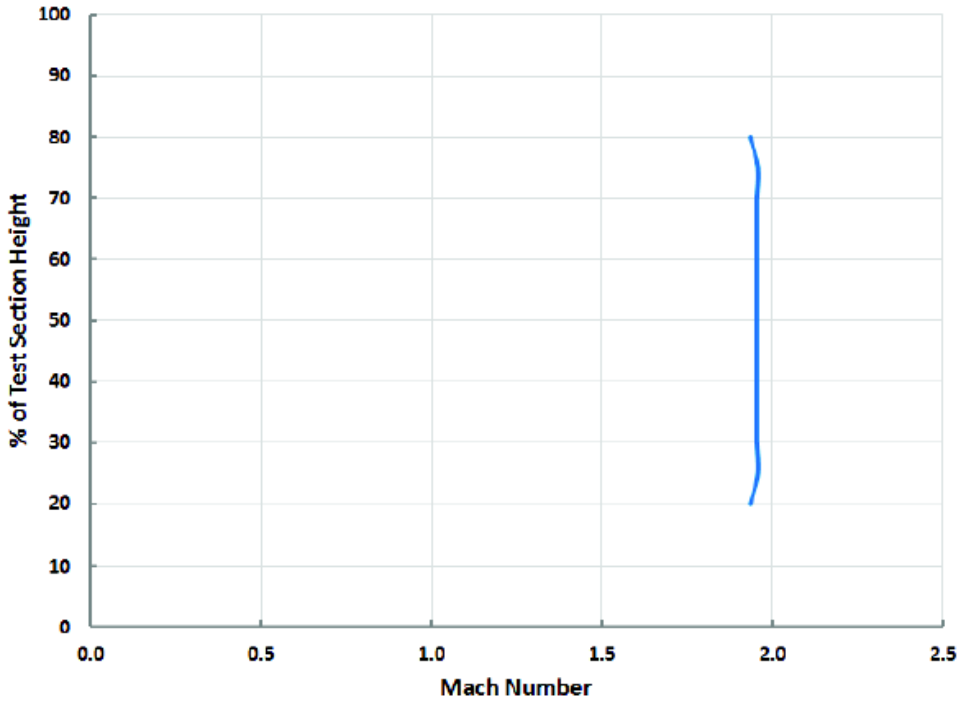

Figure 4.1. Plot of Mach number vs. Test Section Height for Mach 2 nozzle flow survey.

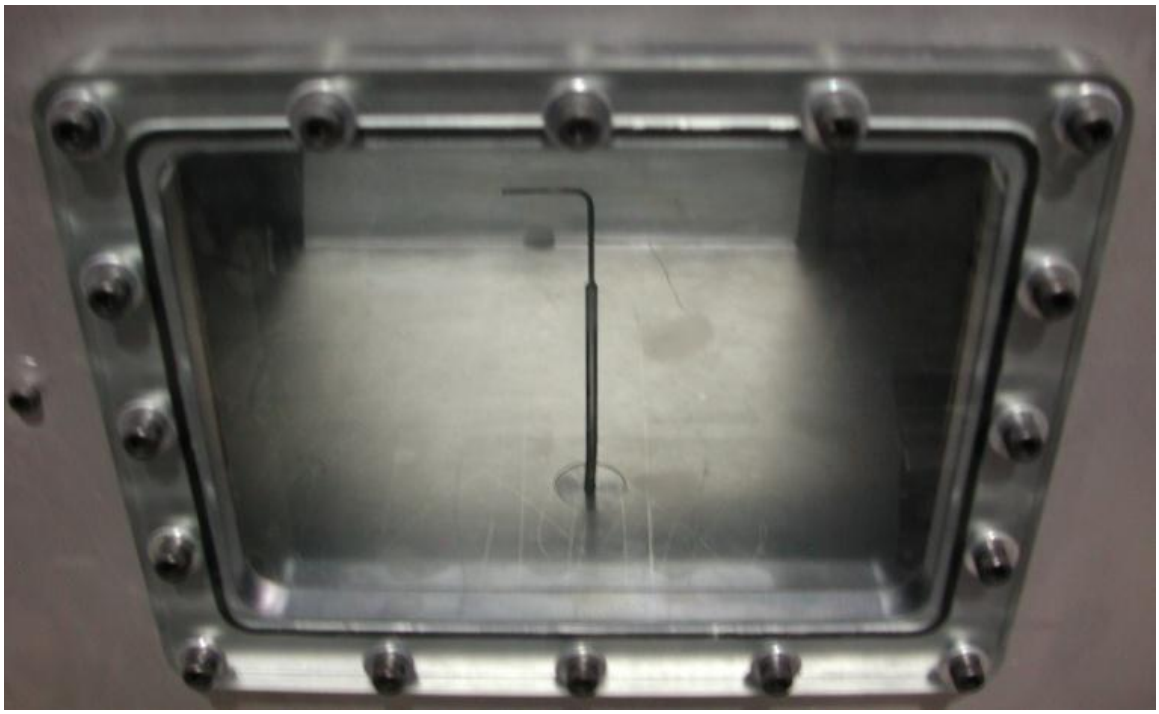

Figure 4.2. Pitot probe within test section during flow survey. The probe is inserted through a port in the floor of the test section, and was traversed over the middle 60% of the test section.

4.3: Experimental Results

Upon completing the wind tunnel shakedown and flow survey, experimental testing of irregular fragments could begin. Fragments are attached to the force balance by means of a fragment adapter piece, which is essentially a supersonic airfoil that attaches to the top of the balance with flat head screws. Due to their irregular shape, not every fragment can have the same orientation of its body axes with respect to the balance axes. Therefore, it is very important to catalog which fragment body axis corresponds to which balance axis. This mapping scheme can be seen below in Table 1 for the two fragments and mount orientations tested.

Table 4.1. Table displaying which fragment body axis corresponds to which balance axis for each fragment and orientation tested.

	Balance +X	**Balance +Y**	**Balance +Z**
Fragment 1	Fragment +X	Fragment -Z	Fragment –Y
Fragment 1 (flipped)	Fragment +X	Fragment +Z	Fragment +Y
Fragment 2	Fragment +Y	Fragment -Z	Fragment +X
Fragment 2 (flipped)	Fragment +Y	Fragment +Z	Fragment -X

Each fragment has a hole drilled through its centroid, and another located 0.75” from the centroid along the fragment’s principal x-axis or y-axis depending on fragment geometry. These holes line up with ones on the fragment adapter piece, and screws are used to hold the fragment in place during testing, since depending on presented area, forces of hundreds of pounds can be placed on the fragment. Fragment 1 can be seen mounted to the force balance in Figure 4.3. The fragment body and balance coordinate systems, and earth fixed coordinate system the data is ultimately converted to and presented in are shown in Figure 4.4.

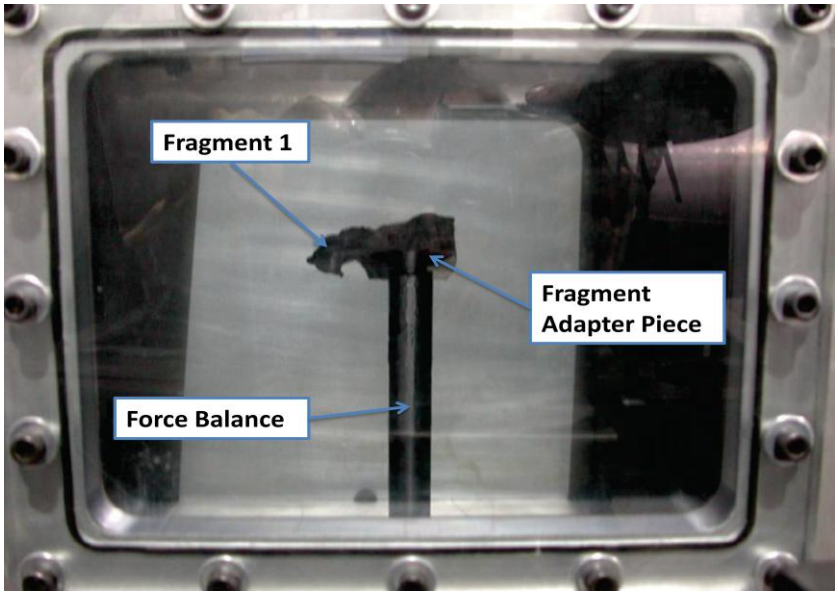

Figure 4.3. Fragment 1 mounted to the force balance in the test section. The small, diamond shaped piece in front of the fragment is the fragment adapter piece. This picture was taken through the window in the side of the test section.

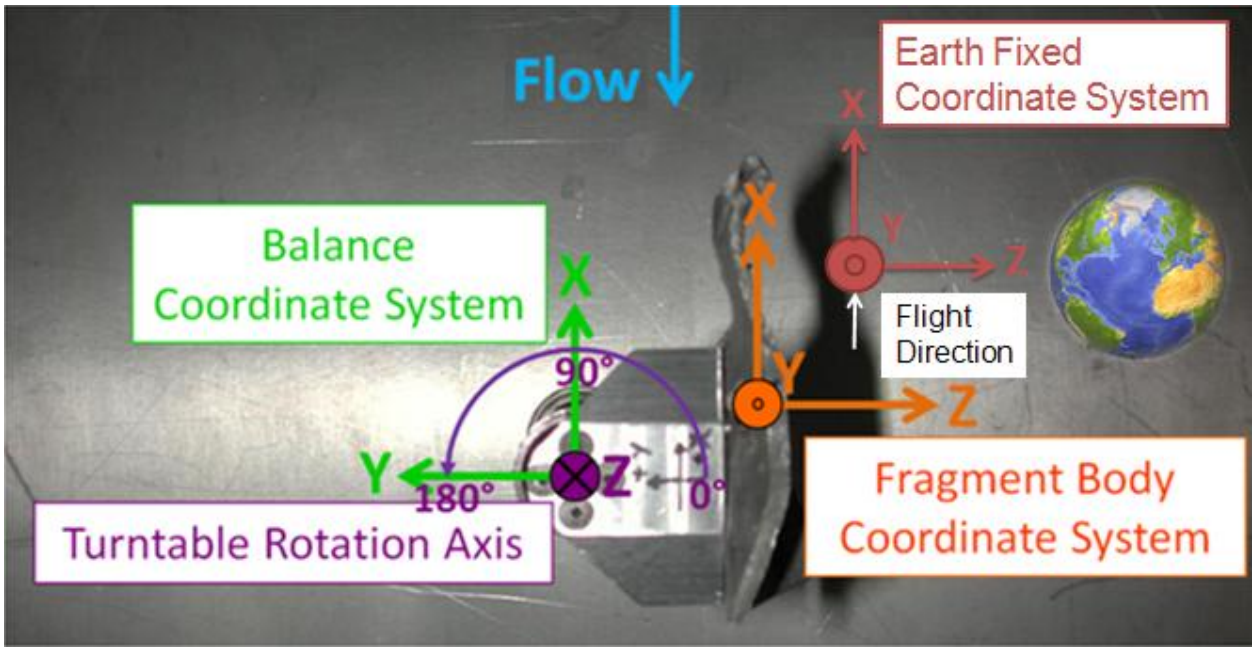

Figure 4.4. Fragment body and balance coordinate systems, and the earth fixed coordinate system which the force data is ultimately converted to and presented in.

Experimental runs were conducted every 10° as the fragment was rotated through a total range of 360°. Instead of performing a full 360° pitch sweep, the fragment was first rotated through 180° as shown above in Figure 4.4. Then, the fragment was flipped 180° about its principal x or y-axis (depending on which is parallel to the balance x-axis), remounted to the balance, and rotated again through the same 180°. This creates an "effective" 360° sweep, since technically two separate 0 to 180° sweeps, at varying bank or elevation angle (depending on whether or not the fragment is mounted with its +x or +y-axis aligned with the fragment x-axis) are performed. If the fragment were simply rotated through a full 360°, throughout the second half of the sweep, the fragment adapter piece would be upstream of the fragment. In this position, shocks coming off the fragment adapter piece would impinge on the fragment and produce undesirable interference effects in the measured forces.

In order to present the fragment force data in a standard form that can be interpreted and replicated, the fragment forces are normalized and converted into the earth fixed coordinate system shown above in Figure 4.4. A flowchart illustrating the experimental procedure and post-processing steps can be seen below in Figure 4.5. During an experimental run the strain gage force balance measures forces along its three principal axes (as shown in Figure 4.4), and the test section total and static pressure, and total temperature are recorded. In addition to determining whether or not the desired Mach number has been established in the test section, these flow measurements are used to normalize the force data by the dynamic pressure in the test section. The force and flow measurements are acquired at a rate of 1,000 samples/second. The data from each run was cropped in order to display only the measurements gathered during the window in

which the tunnel was "started", having a nominal test section Mach number of 2. Prior to conducting experimental runs with a fragment attached, runs were performed over the same range of angles with only the force balance and fragment adapter placed in the test section. This allowed the forces resulting from the presence of these components to be subtracted from experimental runs when a fragment is attached, a common practice generally referred to as a "sting tare." In addition, an instrumentation tare is applied to every single run prior to testing, allowing for the weight of the fragment and strain gage output at zero load to be removed from the force measurements.

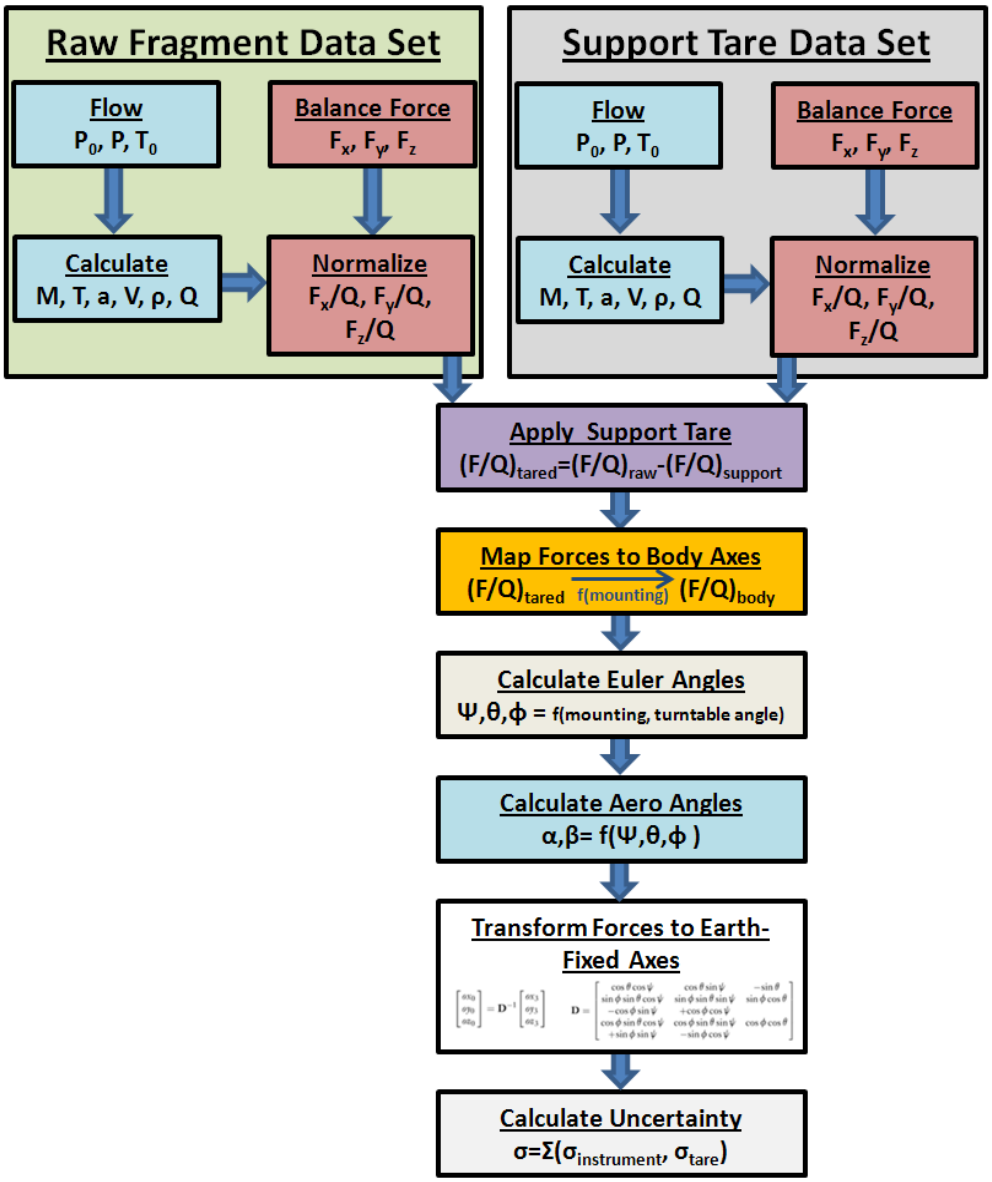

Figure 4.5. Post-processing flowchart of wind tunnel data.

After the support tare has been applied, the forces are converted from the balance coordinate system to their respective fragment coordinates using the mapping scheme shown above in Table 4.1. Euler angles, which represent three composed rotations that transform one reference frame to another, are used to convert the fragment body forces to the earth fixed coordinate system. The Euler angles (azimuth ψ, elevation θ, and bank ϕ) are calculated depending on the fragment mapping and balance pitch angle. The Euler angle conventions can be seen below in Figure 4.6. The subscript 0 corresponds with the earth fixed coordinate system, and the subscript 3 corresponds with the fragment body coordinate system as it is oriented relative to the earth fixed system. The aerodynamic angles are then calculated, in order to be used as the abscissa in the final force data plots. Lastly, the aerodynamic forces are converted from the fragment body coordinate system to the earth fixed coordinate system by multiplying the body force vector by the inverse of the direction cosine matrix D, as shown below in Equations 4.1 and 4.2 (Curtis, 2009). The earth fixed coordinate system is defined with +x is in the direction of flight, +y to the right and tangent to the local horizon, and +z pointing toward the earth, and is equivalent to the fragment body coordinate system of Fragment 1 at a balance pitch angle of 0°, as shown in Figure 4.4.

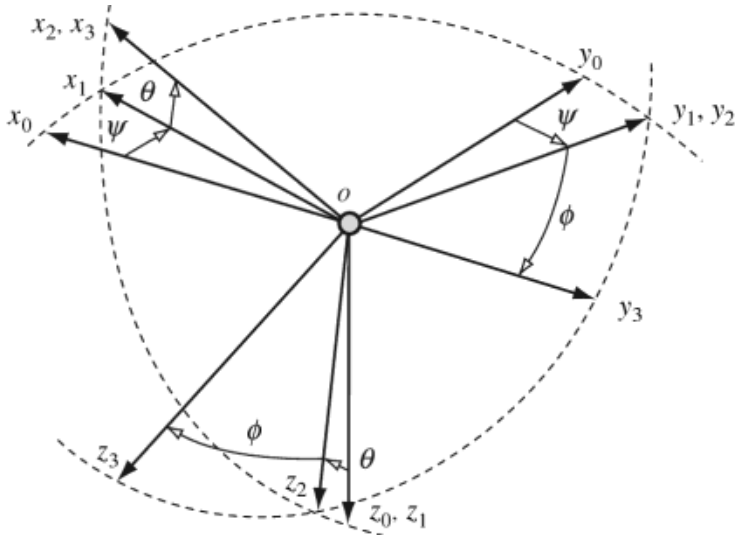

Figure 4.6. Euler angle convention, subscript 0 refers to the earth fixed coordinate system, and subscript 3 refers to the fragment body coordinate system as.(Figure obtained from Aerospace Engineering Desk Reference, Curtis 2009)

$$\begin{bmatrix} ox_3 \\ oy_3 \\ oz_3 \end{bmatrix} = \mathbf{D} \begin{bmatrix} ox_0 \\ oy_0 \\ oz_0 \end{bmatrix}$$

Equation 4.1

$$\mathbf{D} = \begin{bmatrix} \cos\theta\cos\psi & \cos\theta\sin\psi & -\sin\theta \\ \sin\phi\sin\theta\cos\psi & \sin\phi\sin\theta\sin\psi & \sin\phi\cos\theta \\ -\cos\phi\sin\psi & +\cos\phi\cos\psi & \\ \cos\phi\sin\theta\cos\psi & \cos\phi\sin\theta\sin\psi & \cos\phi\cos\theta \\ +\sin\phi\sin\psi & -\sin\phi\cos\psi & \end{bmatrix}$$

Equation 4.2

Plots of the force data, in the earth fixed coordinate system and normalized by dynamic pressure, for Fragments 1 and 2 can be seen below in Figures 4.7, 4.8, 4.9, and 4.10. Photographs of the fragments, taken from above the test section access door, at 0° balance pitch angle can be seen next to their respective force plots. Since Fragment 1 is mounted with its x-axis parallel to the balance x-axis, it is plotted with angle of attack, α, as its abscissa for both its standard orientation (0° bank angle) and "flipped" orientation (180° bank angle). Fragment 2 is mounted with its y-axis parallel to the balance x-axis, and is therefore plotted with sideslip, β, as its abscissa for both its standard orientation (0° elevation angle) and "flipped" orientation (180° elevation angle). For both fragments this equates to two 180° sweeps, one with the fragment body +z axis pointing away from the balance, and the other pointing towards the balance. The lift and drag correspond to the plotted force data by the following relations shown below in Equations 4.3 and 4.4.

$$Lift = \sqrt{F_{ye}^2 + F_{ze}^2} \qquad \textbf{Equation 4.3}$$

$$Drag = -F_{xe} \qquad \textbf{Equation 4.4}$$

From Figures 4.7 and 4.8 it can be seen, for both the standard and "flipped" fragment body orientations of Fragment 1, that the lift force follows a sinusoidal curve, with minimum values at approximately 0, 90, and 180° balance pitch angles. For both orientations, the maximum lift on Fragment 1, approximately 5 in^2, was observed at balance pitch angles of 45° and 135°. The drag force on Fragment 1 follows a smooth curve, with minimum values at 0° and 180°. As expected, the maximum drag force, about 10 in^2, occurs at a balance pitch angle of approximately 90° when the fragment presented area is greatest. In comparing the two plots of Figures 4.7 and 4.8, it can be seen that slightly larger drag forces are observed for the "flipped" orientation (180° bank angle), in which the concave side of the fragment is facing into the direction of flow.

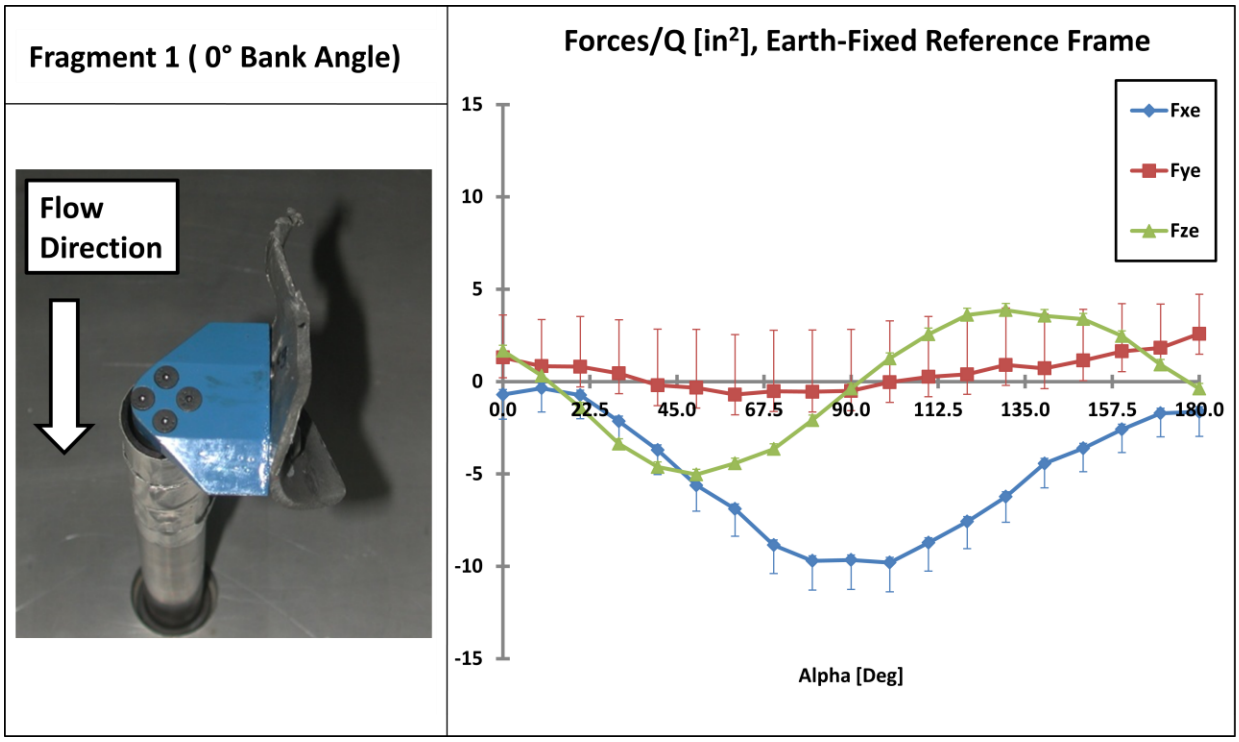

Figure 4.7. Plot of aerodynamic loads on Fragment 1 at Mach 2 and 0° bank angle, normalized as Force/Dynamic Pressure (in^2), in the earth-fixed reference frame.

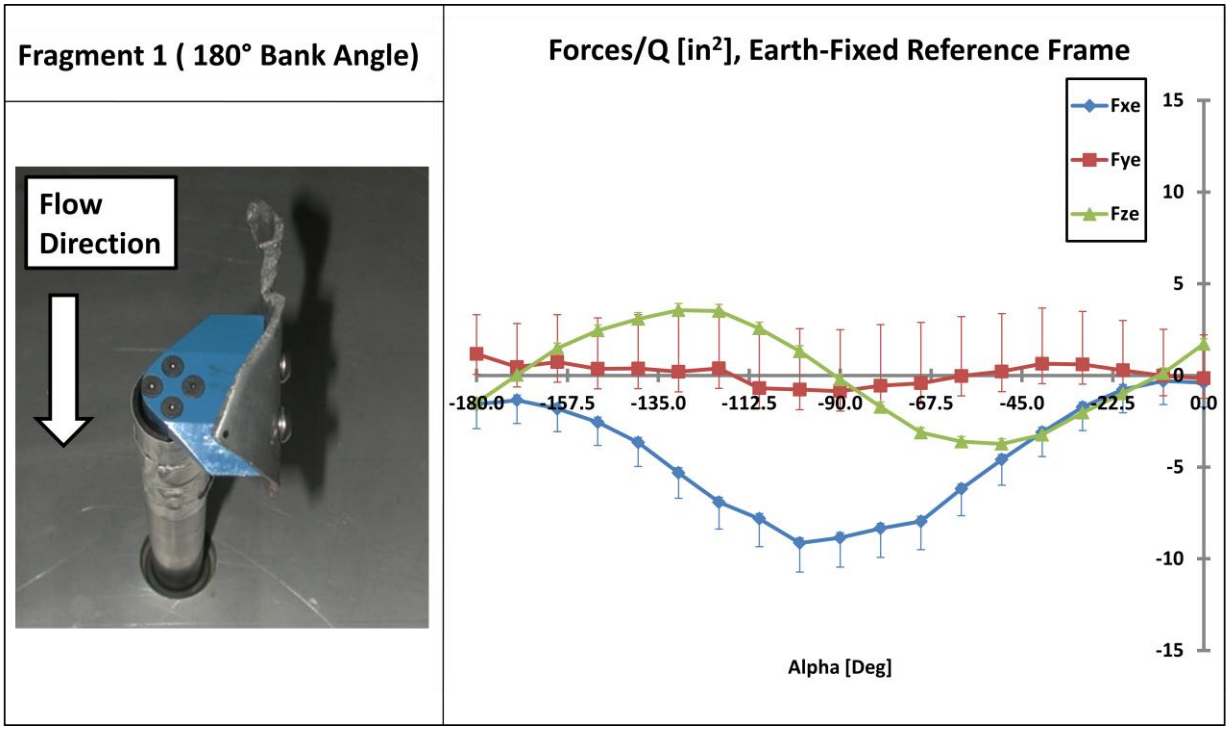

Figure 4.8. Plot of aerodynamic loads on Fragment 1 at Mach 2 and 180° bank angle, normalized as Force/Dynamic Pressure (in^2), in the earth-fixed reference frame.

The force plots for Fragment 2, seen below in Figures 4.9 and 4.10 appear to follow the same trends as Fragment 1. Once again, the lift force follows a sinusoidal curve, and the drag force follows a gradual curve with minimum values at balance pitch angles of 0 and 180°, and a maximum value at 90°. As can be seen in Figure 4.9, the lift and drag on Fragment 2 for the 0° elevation angle case is not as uniform as for the 180° case. This non-uniformity is most likely due to the highly irregular shape of the fragment, since various edges on the fragment become exposed to the flow throughout the 180° pitch sweep. It is interesting to note that the lift force on Fragment 2 in the 180° elevation orientation is approximately twice as much as the 0° elevation angle orientation. In addition, just as for Fragment 1, the drag force on the fragment orientation with the concave side pointing directly into the flow (180° elevation angle) is slightly greater than the orientation which places the convex side (0° elevation angle) into the flow.

The error bars on the plots include both instrument uncertainty and the uncertainty associated with the full range of the support tare (as if the support tare had not been applied). The support tare uncertainty is included in order to increase the confidence in the presented data. Even though care was taken to minimize the effects of the fragment support, at small and large balance pitch angles oblique shocks and expansion waves coming off the fragment adapter piece likely to introduce some loading and/or interfere somewhat with the flow passing over the fragment body. However, at balance pitch angles around 90° the fragment adapter piece is completely shielded by the fragment body. Therefore, the support tare is not as applicable at these pitch angles. Rather than attempting to quantify the interference effects for every balance pitch angle tested, the full range of the support tare is simply included in the uncertainty range. It must also be noted that greater confidence exists in the data for fragments of larger size, since the support tare represents a smaller portion of the overall measured forces.

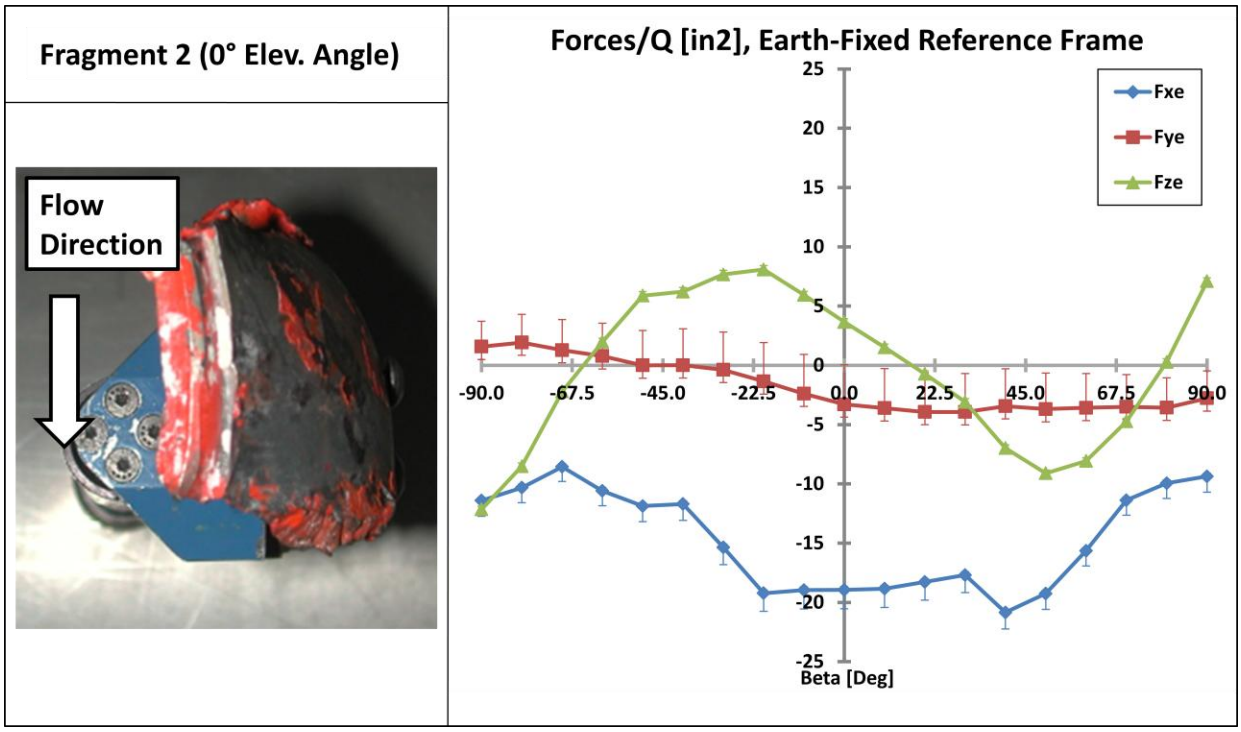

Figure 4.9. Plot of aerodynamic loads on Fragment 2 at Mach 2 and 0° elevation angle, normalized as Force/Dynamic Pressure (in^2), in the earth-fixed reference frame.

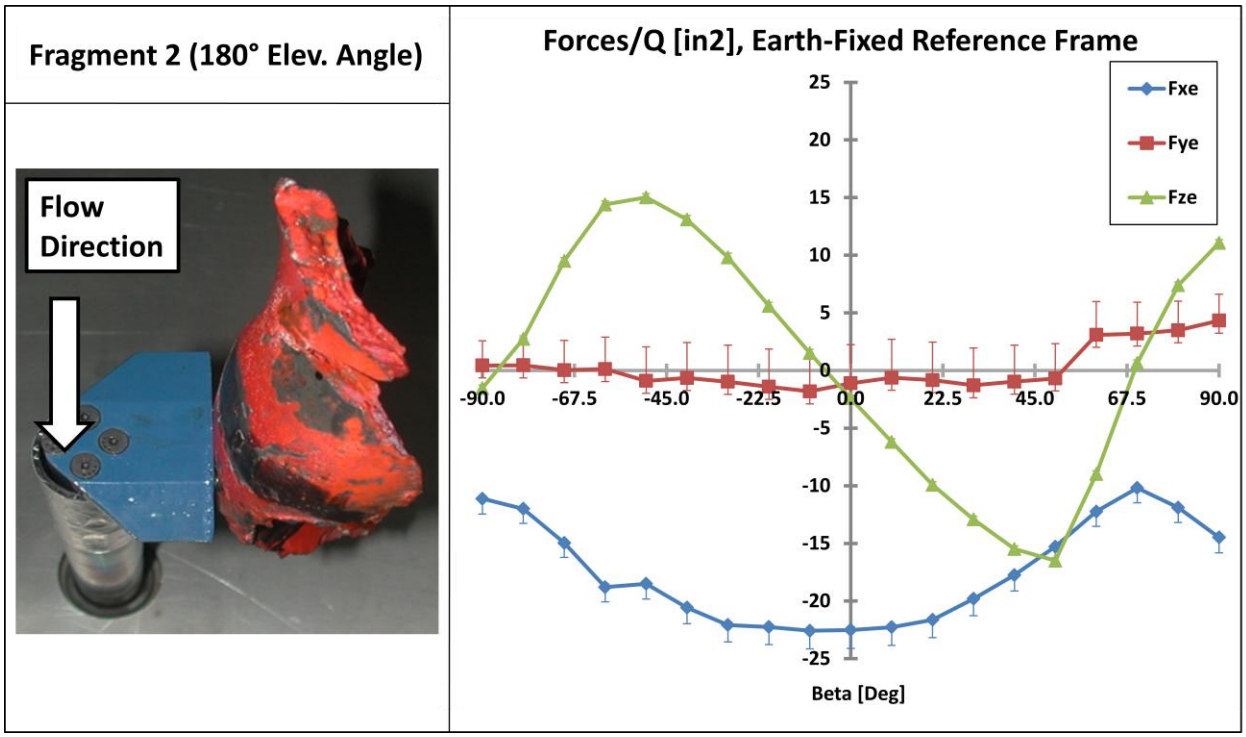

Figure 4.10. Plot of aerodynamic loads on Fragment 2 at Mach 2 and 180° elevation angle, normalized as Force/Dynamic Pressure (in^2), in the earth-fixed reference frame.

Chapter 5.0: Conclusions and Recommendations

Prior to beginning any sort of design on the supersonic wind tunnel, a blowdown wind tunnel analysis model was created in order to investigate the effects of a number of parameters on wind tunnel run time and test section and storage tank test gas properties over time. Input parameters for the model include air storage tank volume and user set pressure, polytropic expansion coefficient, diffuser pressure recovery, ambient temperature and pressure, test section cross sectional area, test section Mach number, and silencer pressure loss. Based on this analysis model, the tunnel run time for a given Mach number, along with the conditions the tunnel would be subjected to for stress analysis calculations, were predicted. The theory behind predicting tunnel run time and required pressure ratio necessary to produce the design Mach number in the tunnel test section is relatively simple. However, due to the complicated phenomena occurring in supersonic tunnels, these predictions often differ significantly from what is seen in reality. Therefore, a great deal of care must be taken in predicting tunnel losses associated with the various wind tunnel components, especially in regards to the diffuser and silencer, in order to ensure a successful design.

Next, the design process of the supersonic wind tunnel components was conducted. Since the only existing components at the wind tunnel facility were two horizontal air storage tanks, mechanical design of the settling chamber, test section, supersonic nozzles, diffuser, and exhaust was necessary. All of the wind tunnel components were designed using SolidWorks. Also, stress analysis for each of these components was conducted using the SolidWorks stress analysis solver. The diverging contour of the supersonic nozzles was determined using a method of characteristics code. Since diffuser pressure recovery can have a significant impact on tunnel run time and efficiency, variable throat diffusers were initially investigated. However, due to their increased cost and complexity, a fixed throat converging-diverging diffuser was ultimately chosen. Aside from cost, the largest constraint in the design of this tunnel was available space within the wind tunnel room. The overall length of the diffuser was limited by the available space in between the test section exit and silencer entrance, resulting in a diffuser much shorter than ideal, ultimately decreasing tunnel performance. If the overall length of the diffuser were increased, it is believed that the flow in the converging section of the diffuser would be decelerated to a much lower Mach number before entering the diffuser throat, leading to a reduction in total pressure loss. CFD simulations of the tunnel flow path including the bellmouth, supersonic nozzles, test section, and diffuser were conducted by Techsburg. In addition to designing wind tunnel components, the control valve and silencer were sized and selected in order to ensure they could withstand the operating conditions of the tunnel. Since these components tend to encompass a large amount of the overall tunnel cost, a great deal of effort should be spent on their selection. Careful sizing of the control valve must be conducted in order to ensure it has a large enough flow capacity for the tunnel operating conditions. In addition, attempts must be made to accurately predict the total pressure loss associated with the

silencer, since this loss has a large impact on the total pressure ratio necessary to produce the design Mach number in the test section.

Once the design of the supersonic wind tunnel was complete, the machining and fabrication of the individual tunnel parts and components could begin. The wind tunnel was assembled as parts were completed by the Techsburg machine shop and outside sheet metal manufacturer. Upon completion of the wind tunnel assembly, shakedown testing was conducted in order to discover whether or not the desired Mach number could be produced in the test section. Also during this time, a valve program which could quickly open the valve in a stable manner and produce uniform Mach 2 flow in the test section was determined. Following shakedown testing, a flow survey was conducted in order to ensure uniform Mach number flow throughout the region which will be occupied by a fragment. In conducting this survey a Pitot tube was inserted through a port in the floor of the test section and traversed vertically. Based on the flow survey, it was determined that within the middle 60% of the test section, the average Mach number was 1.950 and varied by only 0.56%. So, even though the tunnel run time is short, the flow in the test section is remarkably uniform during the time in which Mach 2 flow is sustained. Although the short run time prevents the dynamic pitching of fragments during runs, only a small amount of pressure is drained from the storage tanks over the course of a run. The relatively small loss in storage pressure allows the tanks to be recharged in approximately 15 minutes. Therefore, many experimental runs can be performed in a single day. Since the air storage tanks already operate at their maximum allowable pressure, the only solution to increasing tunnel run time would be do decrease the test section cross sectional area. However, due to the blockage issues associated with supersonic tunnels, decreasing test section size reduces the size of models capable of being tested.

Upon completion of shakedown testing and the flow survey, experimental testing could begin. Two fragments of differing size and shape were mounted to a three-component strain gauge force balance in the test section, and rotated through an "effective", full 360° pitch sweep. Prior to conducting these tests, force data was gathered over the same range of angles with only the force balance and fragment adapter piece placed in the test section. This is a common practice used to subtract the forces associated with the sting/balance from the forces measured when a fragment is mounted to the sting/balance, and is generally referred to as a "sting tare." The full range of this tare was included in the uncertainty of the force data in order to provide for greater confidence, since determining interference effects between the support and fragment is very difficult. The trends of the force data for both of the fragments and their respective mount orientations were very similar. The lift force followed a sinusoidal curve, while the drag force increased gradually from minimum values at 0 and 180° balance pitch angle to a maximum value at 90° pitch angle. This was an expected result since the fragment presented area is generally least at 0 and 180°, and greatest at a balance pitch angle of 90°.

References

Anderson, J.D. *Modern Compressible Flow*. McGraw-Hill, 1982, pp. 39-118.

Bushnell, D. M., Tripi, R. L. *Supersonic Wind Tunnel Optimization*. Presented at the AIAA 14th Aerodynamic Testing Conference, March 1986. AIAA Paper No. 1986-0773.

Curtis, Howard, and Antonio Filippone. *Aerospace Engineering Desk Reference*. San Diego: Butterworth-Heinemann, 2009.

Dayman, Bain Jr. "Blocking in the Supersonic Wind Tunnel." *Journal of the Aeronautical Sciences* 25.4 (1958): 264-65.

Diggins, J. L. *Diffuser Investigations in a Supersonic Wind Tunnel*. NAVORD REPORT 1570. 1951.

Hill, Philip G., Peterson, Carl R. *Mechanics and Thermodynamics of Propulsion*. 2nd ed. Reading, MA: Addison-Wesley, 1992.

Ishikawa K, Nakamura I. *Performance Chart and Optimum Geometries of Conical Diffuser with Uniform Inlet Flow and Free Discharge*. JSME Int Journ, Series II, 32(4): 559-567, 1989.

Japikse, David, and Baines C. Nicholas.*Diffuser Design Technology*. Concepts ETI Inc, 1998, pp. 61-72.

Launius, R. D., Irvine, T. B., Arrington, E. A. *NACA/NASA and the Unitary Wind Tunnel Plan 1945-1965*. Presented at the AIAA 40th Aerospace Sciences Meeting and Exhibit, January 2002. AIAA Paper No. 2002-1142.

McCleskey, Frank. *Drag Coefficients for Irregular Fragments*. NSWC TR 87-89. 1988.

Pinkel, Irving I. *Equations for the Design of Two-Dimensional Supersonic Nozzles*. NACA Rep. no. 907. 1948.

Pope, Alan, and Kennith L. Goin. *High-Speed Wind Tunnel Testing*. New York: John Wiley & Sons, 1965, pp. 1-134.

Schubauer G. B, Spangenberg W. G, and Klebanoff P.S. *Aerodynamic Characteristics of Damping Screens*, NACA TN 2001, 1950.

White, Frank M. "Experimental Duct Flows: Diffuser Performance." *Fluid Mechanics*. 3rd ed. New York: McGraw-Hill, 1994, pp. 384-352.

Appendix A:

Methods and Equations Used in Wind Tunnel Blowdown Analysis Model

This section details the methods and equations of the supersonic wind tunnel blowdown anlaysis model. The inputs of the analysis model can be seen below in Table A.1.

Table A.1. User inputs for supersonic blowdown wind tunnel analysis model.

Model User Inputs	Values Input
Air Storage Tank Volume (gallons)	10,7000
Air Storage Tank Pressure (psig)	217
Polytropic Expansion Coefficient	1.4
Diffuser Pressure Recovery	0.9
Ambient Temperature (Storage Tank Temp.) (°F)	70
Ambient Pressure (psi)	13.6
Test Section Cross Sectional Area (in^2)	400
Test Section Mach Number	2
Silencer Pressure Loss (psi)	18

Air Storage Tank Initial Conditions. The air storage tank initial conditions are determined with knowledge of the user set tank initial pressure, and ambient temperature of the wind tunnel room, which is assumed to be equivalent to the storage tank stagnation temperature. With the above values, the density and mass of the air in the air storage tanks can be determined using the ideal gas equation shown below.

$$\rho_0 = \frac{p_0}{RT_0} \qquad \textbf{Equation A.1}$$

With knowledge of the storage tank volume, the mass of the air in the tanks can be determined from the following equation.

$$\mathcal{M} = \left(\frac{p_0}{RT_0}\right)(\mathcal{V}) \qquad \textbf{Equation A.2}$$

Test Section Initial Conditions. Knowing the desired test section Mach number, if a normal shock were to occur at this Mach number, the resulting downstream Mach number can be determined from the following normal shock relation.

$$M_2 = \sqrt{\frac{(\gamma-1)(M_1^2+2)}{2\gamma M_1^2-(\gamma-1)}} \qquad \textbf{Equation A.3}$$

Next, the stagnation pressure ratio across this normal shock can be determined from the equation shown below.

$$\frac{p_{02}}{p_{01}} = \left(\frac{1+\frac{\gamma-1}{2}M_2^2}{1+\frac{\gamma-1}{2}M_1^2}\right)^{\left(\left(\frac{\gamma}{\gamma-1}\right)\left(\frac{2\gamma M_1^2-(\gamma-1)}{\gamma+1}\right)\right)} \qquad \textbf{Equation A.4}$$

The test section stagnation pressure for a given test section Mach number can then be determined from the following equation.

$$p_{0\_TS} = \frac{(p_{amb}+p_{0\_SL})}{r\left(\frac{p_{02}}{p_{01}}\right)} \qquad \textbf{Equation A.5}$$

Where, r is the diffuser pressure recovery and p_{0_SL} is the silencer total pressure loss.

The static pressure and temperature within the test section can then be determined from the isentropic Mach number relations shown below.

$$\frac{p_{0\_TS}}{p_{TS}} = \left(1 + \frac{\gamma-1}{2}M^2\right)^{\gamma/\gamma-1} \qquad \textbf{Equation A.6}$$

$$\frac{T_{0\_TS}}{T_{TS}} = \left(1 + \frac{\gamma-1}{2}M^2\right) \qquad \textbf{Equation A.7}$$

The test section static density can then be calculated using the ideal gas law shown in Equation A.8 below, just as for the density of the air in the storage tanks.

$$\rho_{TS} = \frac{p_{TS}}{RT_{TS}} \qquad \textbf{Equation A.8}$$

After determining the static properties of the air in the test section, the velocity and mass flow rate can be found using the equations below.

$$V = M\sqrt{\gamma RT} \qquad \textbf{Equation A.9}$$

$$\dot{m}_{TS} = \rho_{TS}A_{TS}V \qquad \textbf{Equation A.10}$$

Air Storage Tank Conditions Over Time. In order to create a more accurate representation of the percent of air in the tank vs. time, losses from the tank to the valve through the 12" pipe were included. These losses are assumed to be the dynamic pressure through the 12" pipe, through which the flow is assumed to be choked.

The percent of air remaining in the tank over time was determined from the equation shown below.

$$\%\ of\ Air\ Remaining\ in\ Storage\ Tanks = \frac{\left(p_{0\_tank}-\left(p_{0_{TS}}+Losses\right)\right)}{\left(p_{0\_tank\_init}-\left(p_{0_{TS}}+Losses\right)\right)} \qquad \textbf{Equation A.11}$$

The mass of air remaining in the storage tanks over time can then be calculated from the following equation.

$$\mathcal{M}_2 = \mathcal{M}_1 - \left(\dot{m}_{TS}(Chosen\ Time\ Step)\right) \qquad \textbf{Equation A.12}$$

The density of the air remaining in the storage tanks can then be determined using the above value of mass remaining and total air storage tank volume.

$$\rho_2 = \frac{\mathcal{M}_2}{\mathcal{V}} \qquad \textbf{Equation A.13}$$

Using isentropic relations the change in tank pressure and temperature over time can be calculated using the equations below. Since the run time of the tunnel is so short, the polytropic expansion coefficient can be assumed to be adiabatic.

$$p_{02} = (p_{01})\left(\frac{\rho_{02}}{\rho_{01}}\right)^{polytropic\ expansion\ coefficient} \qquad \textbf{Equation A.14}$$

$$T_{02} = (T_{01})\left(\frac{p_{02}}{p_{01}}\right)\left(\frac{\rho_{01}}{\rho_{02}}\right) \qquad \textbf{Equation A.15}$$

Test Section Conditions Over Time. During the time when the test section is at its desired Mach number, the stagnation and static pressure within the test section remain constant. The static temperature over time can be determined using isentropic Mach number relation just as in calculating the initial test section static temperature.

$$T_{TS} = \frac{T_{0\_tank}}{1+\frac{\gamma-1}{2}M^2} \qquad \textbf{Equation A.16}$$

The velocity of the air over time can then be determined using the speed of sound equation shown below.

$$V = M\sqrt{\gamma R T_{TS}} \qquad \textbf{Equation A.17}$$

Lastly, the mass flow rate over time can be calculated from the following equation.

$$\dot{m}_2 = \dot{m}_1\sqrt{\frac{T_{01\_tank}}{T_{02\_tank}}} \qquad \textbf{Equation A.18}$$

Appendix B: Wind Tunnel Stress Analysis

In order to ensure the wind tunnel components could withstand the forces placed on them during experimental testing, stress analysis was performed on the settling chamber, test section, diffuser, and exhaust using the SolidWorks stress analysis solver. Within the solver one can fix faces and edges of a body, apply forces, and choose material properties to determine a parts factor of safety. The SolidWorks solver is a linear static analysis solver, and therefore makes the linearity, elasticity, and static assumptions. In order to assume linearity the greatest stress placed on the part/component must be within the linear range of the stress-strain curve, and the maximum displacement must be considerably less than the thickness of the part. The elasticity assumption states that the part must return to its original shape once the loads are removed. Lastly, in order to make the static assumption the loads must be applied slowly until they reach their full magnitude.

Settling Chamber Stress Analysis. The wide angle diffuser and settling chamber were fabricated from 0.25 inch thick, plain carbon steel, sheet metal. Stress analysis was conducted using SolidWorks in order to ensure the above wind tunnel components would not fail under operating conditions. Through the use of the wind tunnel blowdown analysis model discussed above, the maximum stagnation pressure within the tunnel for the desired Mach numbers to be tested was determined to be approximately 50 psi. Since the flow within the wide angle diffuser and settling chamber is moving at a relatively low velocity when compared to that in the test section, the stagnation pressure listed above was used in their stress analysis calculation. A 50 psi load was applied to the inner walls of the wide angle diffuser and settling chamber, while the flanges on the upstream and downstream ends were held fixed. Stress analysis was also conducted on the blind flange at the end of the settling chamber. The material of the blind flange is 6061-T6 aluminum alloy, since a steel blind flange of the same size would weigh a considerably larger amount. In addition to the 50 psi load on the inner face of the blind flange, a 27,000 N thrust force was placed on the outer face. This force was placed over an area equivalent to the footprint of the angle plates which attach the test section to the settling chamber, and accounts for the thrust resulting from the supersonic nozzles. Based on the SolidWorks stress analysis solver, the factor of safety for the wide angle diffuser and settling chamber was estimated to be 6.09. The blind flange was estimated to have a factor of safety of 2.54. The blind flange has the lowest factor of safety of the entire tunnel circuit. However, in the stress analysis calculation it was constrained around its outer edge, a conservative fixture. In reality, the blind flange is attached to the settling chamber exit, which has a 5.75” wide flange, by 44 ¾” bolts. Stress contour images of the settling chamber and blind flange obtained from the stress analysis solver can be seen below in Figure B.1.

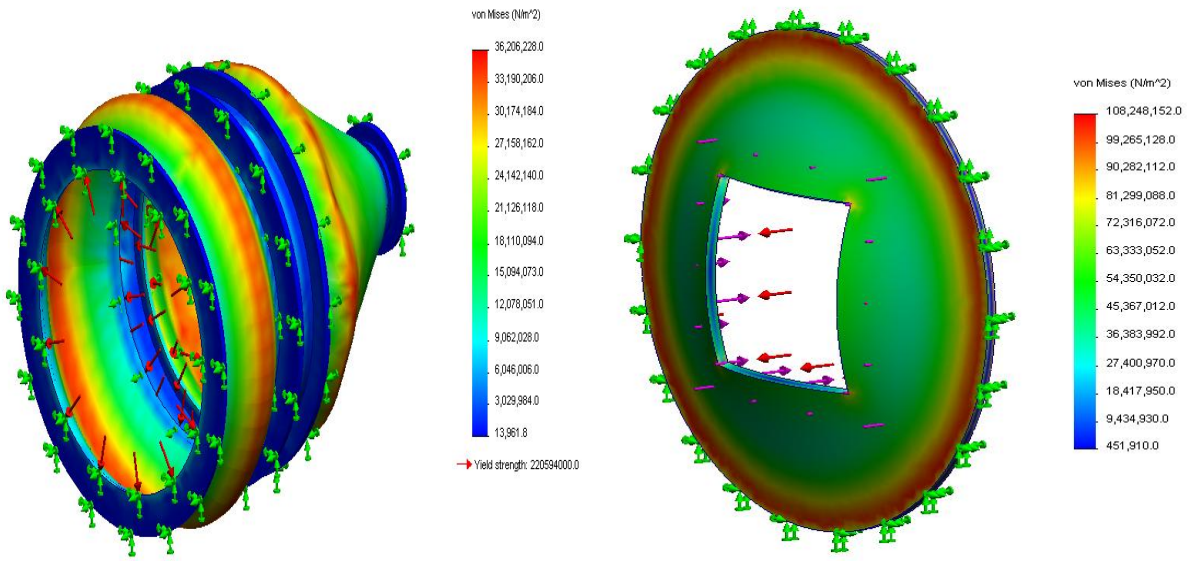

Figure B.1. Stress contours of the wide angle diffuser/settling chamber (left) and blind flange (right). The deformation of the components is extremely exaggerated in the image produced by the stress analysis solver, and is very small in magnitude.

Test Section Stress Analysis. All of the test section and balance enclosure walls, flanges, and doors are made of 6061-T6 aluminum. In order to determine the stress on the test section during testing, the SolidWorks solver was once again used. During the period of time in which the tunnel is started at the desired Mach number, the pressure within the test section is near vacuum. However, before the normal shock has passed through the test section and during tunnel unstart, the pressures are much higher. Therefore, the maximum stagnation pressure obtained from the blowdown spreadsheet, approximately 50 psi, is applied to the inner walls of the test section in order to determine its factor of safety. Stress analysis was also conducted under the conditions of vacuum in the test section in order to determine its factor of safety while the tunnel is started. The test section factors of safety under the two conditions analyzed were determined to be 4.08 and 14.7. Stress contour images of the two conditions can be seen below in Figure B.2.

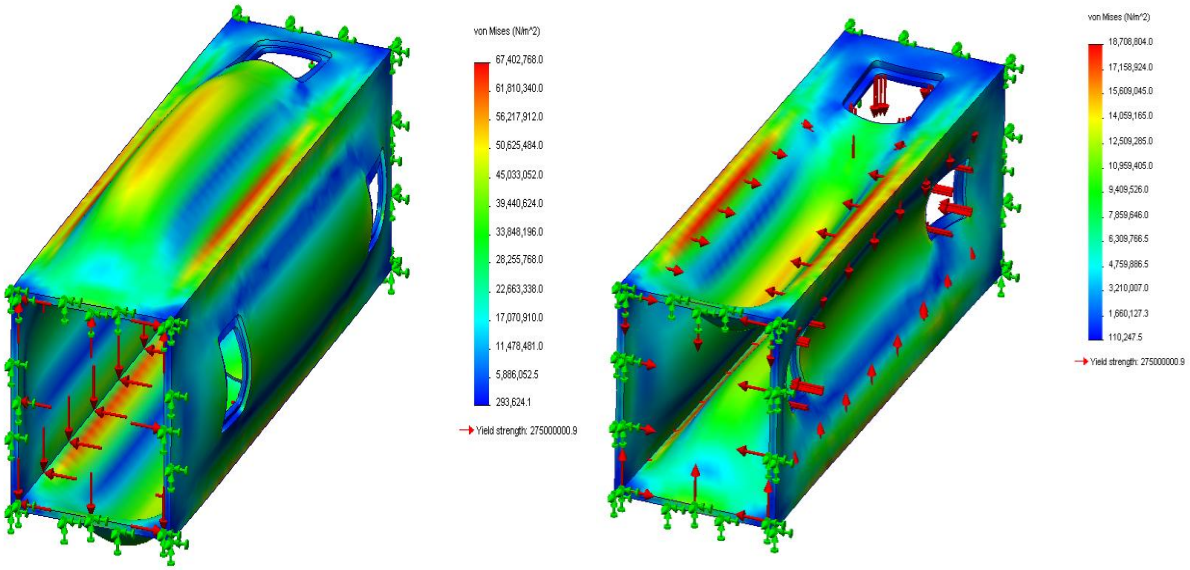

Figure B.2. Stress contours of the test section under conditions of a 50 psi load applied to its inner walls (left) and vacuum (right). The deformation of the test section is extremely exaggerated in the image produced by the stress analysis solver, and is very small in magnitude.

In order to ensure the test section window and access doors could withstand the tunnel operating conditions, stress analysis was also conducted on these parts. The 50 psi maximum stagnation pressure load was applied to the inner faces of the test section window and access door, while the faces which mate with the slots in the test section walls were held fixed. The factors of safety of the window and test section access door were determined to be 39.58 and 5.56. Images of the stress contours for the window and access door can be seen below in Figure B.3.

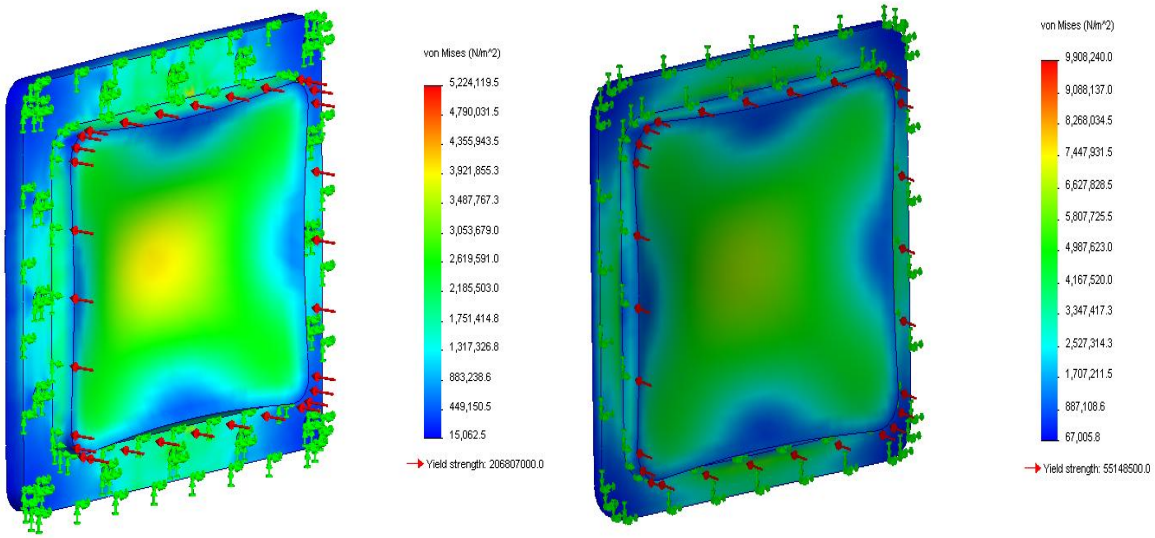

Figure B.3. Stress contours of the test section window (left) and access door (right) under conditions of a 50 psi load applied to their inner face.

Diffuser Stress Analysis. The converging and diverging sections of the diffuser were fabricated from 0.25 in. thick, plain carbon steel sheet metal. Stress analysis was conducted using the SolidWorks stress analysis solver in order to make sure the diffuser could withstand the operating conditions of the tunnel with a suitable factor of safety. In conducting the stress analysis the maximum stagnation pressure of 50 psi was placed on the inner walls of the diffuser as the flanges on each were held fixed. During tunnel operation the pressure in the diffuser will be lower than this value. However, cases exist in which this pressure could occur. Under the 50 psi pressure load it was determined that the diverging section of the diffuser had a factor of safety of 9.89. Accurately modeling the geometry of the converging section of the diffuser in the stress analysis solver proved difficult, and a definitive factor of safety for this part was not determined. However, since the two sections of the diffuser are similar in design, based on the factor of safety obtained for the diverging section, it is assumed that the converging section could withstand the operating conditions of the tunnel. A stress contour image of the diffuser output by the SolidWorks solver can be seen below in Figure B.4.

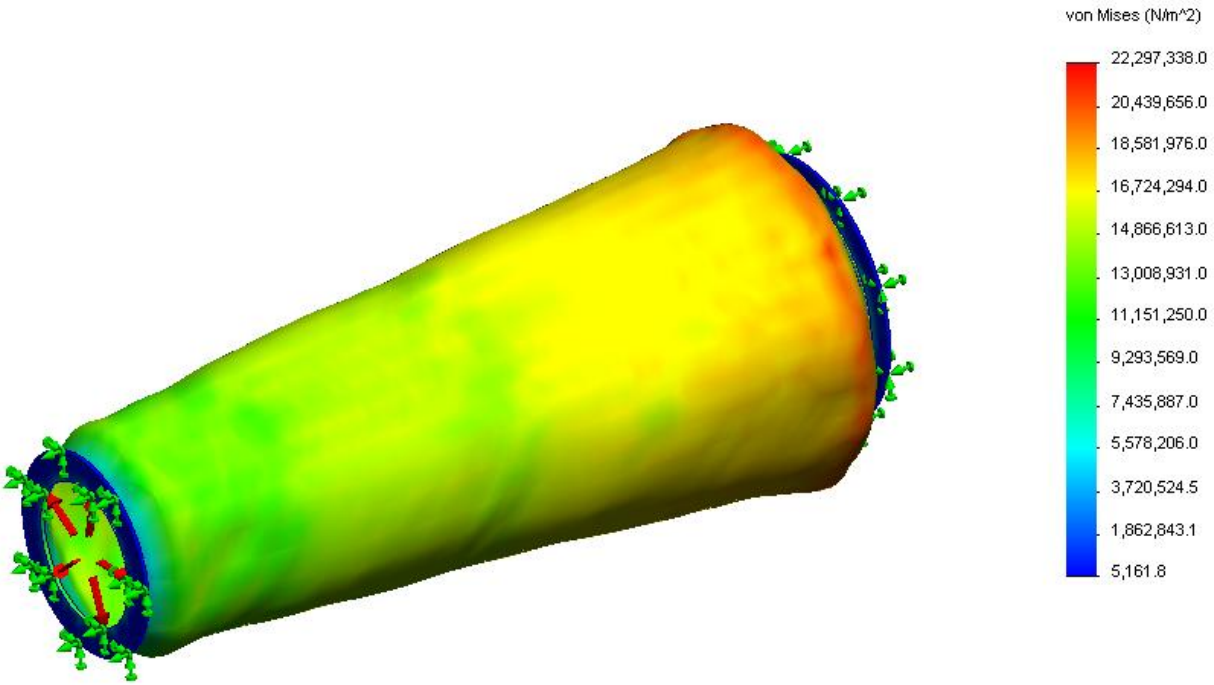

Figure B.4. Stress contour image of the diverging section of the diffuser. The deformation of the diffuser is extremely exaggerated in the image produced by the stress analysis solver, and is very small in magnitude.

Exhaust Stress Analysis. The exhaust was also fabricated from 0.25" thick, plain carbon steel sheet metal. Once again the SolidWorks stress analysis solver was used in order to investigate the stresses resulting from the force and pressure loads on the exhaust stack during tunnel operation. In the stress analysis solver the maximum stagnation pressure of 50 psi was applied to the inner walls of the exhaust, and a 5,000 lbf tension load was placed on the upper edges of the inner exhaust pipe and shroud pipe. This tension load represents the drag force on

the exhaust resulting from the momentum of the air leaving the wind tunnel circuit. Under these pressure and tension loads the factor of safety on the exhaust was determined to be 6.67. A stress contour image of the exhaust produced by the SolidWorks solver can be seen below in Figure B.5.

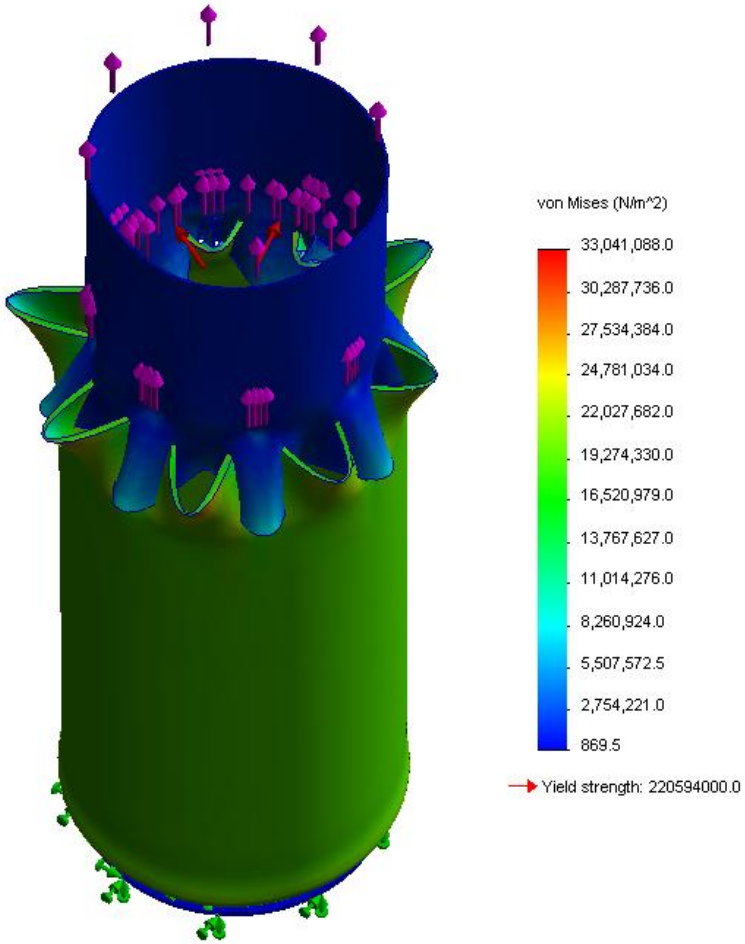

Figure B.5. Stress contour of supersonic wind tunnel exhaust under pressure and drag loads. The deformation of the exhaust is extremely exaggerated in the image produced by the stress analysis solver, and is very small in magnitude.

Appendix C: Uncertainty Analysis

The following section discusses the uncertainty of the parameters measured during wind tunnel experimental runs. The instrumentation used in the experimental runs, and their respective uncertainties can be seen below in Table C.1.

Table C.1. Errors associated with instrument uncertainty.

Measurement(s)	Instrument	Instrument Uncertainty
Test Section Stagnation Pressure, p_{0_TS}	Validyne Pressure Transducer 0-125 psid	+/- 0.625 psi
Test Section Static Pressure, p_{TS}	Validyne Pressure Transducer 0-20 psid	+/- 0.1 psi
Air Storage Tank Stagnation Pressure, T_{0_tank}	Omega TAC80B K-type Thermocouple to Analog Converter	+/- 6.1°F
Force Measurements: F_{xe}, F_{ye}, F_{ze}	Three-Component Strain Gauge Force Balance (uncertainties are for balance principal axes)	+/- 2.5 lbf (x-axis) +/- 2.5 lbf (y-axis) +/- 10 lbf (z-axis)

In order to determine the Mach number of the flow in the test section, two pressure transducers are used to measure total and static pressure. The error in determining Mach number obtained by using static pressure and total head is given by the relation shown below in Equation C.1. A k-type thermocouple was used to measure the air storage tank stagnation temperature, which is assumed to be equivalent to the test section stagnation temperature. Once the test section Mach number has been determined, the measured storage tank temperature can be used along with the isentropic Mach number relation shown above in Equation A.7 to determine the test section static temperature. Therefore, the errors associated with the static temperature calculation are compounded by the errors associated with the Mach number and stagnation temperature as shown in Equation C.2 below. The velocity of the air in the test section is calculated with knowledge of the Mach number and static temperature. Therefore, the error in the velocity calculation is compounded by the error associated with these parameters, shown by the expression in Equation C.3 below. Lastly, the static density of the flow in the test section is calculated using the ideal gas law along with the measured and calculated static pressure and temperature. The error associated with the static density value is compounded by the errors resulting from the Mach number, and static temperature, as shown in Equation C.4.

$$\delta M = M\left(\frac{1+[(\gamma-1)/2]M^2}{\gamma M^2}\left(\frac{\partial p_{01}}{p_{01}} - \frac{\partial p}{p}\right)\right) \qquad \textbf{Equation C.1}$$

$$\delta T = \sqrt{\left[\left(\frac{\partial T}{\partial T_0}\right)\delta T_0\right]^2 + \left[\left(\frac{\partial T}{\partial M}\right)\delta M\right]^2} \qquad \textbf{Equation C.2}$$

$$\delta V = \sqrt{\left[\left(\frac{\partial V}{\partial T}\right)\delta T\right]^2 + \left[\left(\frac{\partial V}{\partial M}\right)\delta M\right]^2} \qquad \textbf{Equation C.3}$$

$$\delta \rho = \sqrt{\left[\left(\frac{\partial \rho}{\partial M}\right)\delta M\right]^2 + \left[\left(\frac{\partial \rho}{\partial T_0}\right)\delta T_0\right]^2 + \left[\left(\frac{\partial \rho}{\partial T}\right)\delta T\right]^2} \qquad \textbf{Equation C.4}$$

The maximum propagated uncertainties in Mach number, test section static temperature, velocity, and density can be seen below in Table C.2. All of the uncertainty calculations were linearized for Mach 2 flow. The maximum propagated uncertainty of the test section static temperature measurement is mainly due to the error associated with the k-type thermocouple. Also, while the test section velocity uncertainty may appear large, it is only about 1% of the roughly 500 m/s flow generated in the test section during experimental runs.

Table C.2. Maximum propagated uncertainty.

Calculated Parameter	Maximum Propagated Uncertainty
Test Section Mach Number	+/- 0.003
Test Section Temperature	+/- 3.355 °F
Test Section Velocity	+/- 4.328 m/s
Test Section Density	+/- 0.009 kg/m^3